Article:

Liu, K., Yang, P. orcid.org/0000-0002-8553-7127, Wang, R. et al. (3 more authors) (2023) Observer-based adaptive fuzzy finite-time attitude control for quadrotor UAVs. IEEE Transactions on Aerospace and Electronic Systems, 59 (6). pp. 8637-8654. ISSN 0018-9251

https://doi.org/10.1109/TAES.2023.3308552

Observer-Based Adaptive Fuzzy Finite-Time Attitude Control for Quadrotor UAVs

Kang Liu, *Member, IEEE*, Po Yang, *Senior Member, IEEE*, Rujing Wang, Lin Jiao, *Member, IEEE*, Tao Li, *Member, IEEE*, and Jie Zhang

***Abstract*—This study presents an observer-based adaptive fuzzy finite-time attitude control strategy for quadrotor unmanned aerial vehicles (UAVs). To estimate the information of angular velocity with the finite-time property, an adaptive neural network observer is first developed. Subsequently, an adaptive fuzzy logic system (FLS)-based nonsingular fast terminal sliding mode controller is proposed to compensate for the lumped disturbance and adjust the control gain online. To cope with the input saturation, an auxiliary system without the boundedness of the saturation difference is constructed. The theoretical analysis proves that all the system signals are bounded and the tracking errors can converge to small neighbourhoods in finite time. Finally, comparative simulations and experiments are performed to manifest the feasibility and superiority of the proposed control strategy, in terms of strong robustness, singularity avoidance, free-chattering, fault tolerance, and saturation attenuation.**

***Index Terms*—Attitude control, finite-time convergence, fuzzy logic system (FLS), input saturation, quadrotor UAVs.**

I. Introduction

In recent years, quadrotor unmanned aerial vehicles (UAVs) have been widely applied in various fields [1]–[5] due to some distinct advantages such as hovering capability, simple structure, and vertical take-off and landing. However, there are many difficulties such as the complex atmosphere, high nonlinearity, under-actuation, and various disturbances [6]–[9]. The above difficulties greatly increase the challenge of the controller design and reduce the dynamic performance. As we know, the accuracy of attitude control directly affects the accuracy of position control, so how to realize the high performance of attitude control is the top priority.

Nowadays, many control strategies have been developed [10]–[15], [17]–[22]. Due to its fast response and strong robustness, the SMC scheme was designed in [10] to compensate for various uncertainties, but large control gain causes severe chattering. To improve the performance of SMC, the study [2] presented an adaptive SMC-based observer, but the disturbance's derivative is required to be bounded. Attributed to the strong approximation ability, radial basis function neural networks (RBFNNs) show remarkable performance for nonlinear systems [11]. An adaptive NN-based dynamic surface control (DSC) policy was proposed to solve the "*exponential explosion*" problem [12]. Tripathi *et al.* [13] designed a disturbance observer (DO)-based SMC and conducted the experiments to verify its validity. Fang's team presented a new NN-based hybrid mode-switching controller for the flapping wing aerial vehicle [14]. As an alternative intelligence method, fuzzy logic system (FLS) can work reasonably well in the face of nonlinear systems [15]–[19]. Besides, FLS provides an effective *human-interpretable* solution that is very easy to understand, especially from the perspective of laypersons. In [19], the *authors* proposed a T-S fuzzy-based event-triggering attitude control for the spacecraft systems to reduce the communication burden. Ma *et al.* [20] presented a hybrid flight controller for unmanned helicopters, where the FLS was constructed to cope with the parametric uncertainties. The fuzzy SMCs were proposed to realize the chattering attenuation and improve the disturbance rejection capability [17], [21], [22]. Although the accurate system dynamics is unnecessary, many logic rules are required for the fuzzy controller design, which would lead to structural complexity and computational pressure. As a result, there remains an ongoing challenge to investigate an adaptive fuzzy approximation control with a simpler fuzzy structure and fewer logic rules.

Recently, the finite-time control has attracted considerable attention [23]–[25]. Its primary advantage is that the system convergence can be guaranteed in finite time instead of infinite time. In [26], a linear-quadratic regulation attitude controller was presented, but it may be impossible to realize the desired control effect for the quadrotor UAV in the presence of high

This work was supported in part by the Innovate UK under Grant 107462, Grant 10002902, and Grant 10050919, in part by the STFC: Sustainable Food Network under Grant 2892395, and in part by the National Natural Science Foundation of China under Grant 62173137, Grant 52172403, and Grant 31671586. *(Corresponding authors: Po Yang; Tao Li.)*

Kang Liu is with the Department of Computer Science, University of Sheffield, Sheffield S10 2TN. U.K., the Institute of Intelligent Machines, Hefei Institutes of Physical Science, Chinese Academy of Sciences, Hefei 230031, China, and also with the Department of Automation, University of Science and Technology of China, Hefei 230026, China (e-mail: xinxilk@mail.ustc.edu.cn).

Po Yang is with the Department of Computer Science, University of Sheffield, Sheffield S10 2TN, U.K.. (po.yang@sheffield.ac.uk).

Rujing Wang is with the Institute of Intelligent Machines, Hefei Institutes of Physical Science, Chinese Academy of Sciences, Hefei 230031, China, and also with the Department of Automation, University of Science and Technology of China, Hefei 230026, China (e-mail: rjwang@iim.ac.cn).

Lin Jiao is with the School of InterNet, Anhui University, Hefei 230031, China, and also with the Institute of Intelligent Machines, Hefei Institutes of Physical Science, Chinese Academy of Sciences, Hefei 230031, China, (e-mail: ljiao@ahu.edu.cn).

Tao Li is with the College of Railway Transportation, Hunan University of Technology, Zhuzhou 412007, China, and also with the Department of Computer Science, University of Sheffield, Sheffield S10 2TN. United Kingdom. (e-mail: litao@hut.edu.cn).

Jie Zhang is with the Institute of Intelligent Machines, and Hefei Institutes of Physical Science, Chinese Academy of Sciences, Hefei 230031, China, (e-mail: zhangjie@iim.ac.cn).

nonlinearity. Moreover, it is less robust and has high sensitivity to unanticipated disturbances. To solve these difficulties, a terminal SMC (TSMC), which adopts a nonlinear surface to replace a linear surface, was presented to realize the finite-time convergence [27], [28]. In contrast to the linear SMC (LSMC), the TSMC has a slower convergence speed and an inevitable singularity. Hence, fast TSMC (FTSMC) [29] and nonsingular TSMC (NTSMC) [30] were proposed for the quadrotor attitude system. However, individual FTSMC [29] or NTSMC [30] schemes cannot handle above two disadvantages in the TSMC. To solve the above two disadvantages, some nonsingular FTSMCs (NFTSMCs) were presented in [9], [31]–[34]. In [9], an adaptive NFTSMC was developed to obtain the desired performance. Xu *et al.* [33] studied a fault-tolerant control (FTC) method based on NFTSMC to achieve strong robustness and fast response. Nevertheless, the chattering problem is difficult to avoid. To this end, several solutions such as the boundary layer technique [29], [31], continuous controller [10], [27], and observer/approximator [25], [35], have been developed. Although these approaches are constructive, they would lose the fast finite-time nature, and there is just theoretical assurance for the control precision. These important requirements correspond to our goal.

Most attitude controllers require the acquirability of angular velocity. However, it is difficult to measure accurately due to sensor failure and measurement noise, and it costs expensive expenses to install extra velocity sensors. Hence far, many works have been deeply studied to obviate this problem [23], [37]–[42]. The motion capture system [37] was used to numerically estimate the velocity signals. However, the obtained velocity signals contain the noises and errors and therefore cannot be used to make rigorous stability analysis. By applying the immersion and invariance technique, an exponentially convergent velocity observer was designed for mechanical systems, but it ignores the unknown parameters and disturbances [38]. Even though the velocity estimation is a critical issue in the quadrotor UAV, the key is to consider the existence of unknown parameters and external disturbances in the design of the state observer. The finite-time observer was presented via high-order sliding mode mechanism [23] to detect the angular velocity, but it requires the boundedness of the disturbance and its first-order derivative. To solve this challenge, in [39] and [40], the *authors* designed a state observer-based FLS/NN, but the finite-time convergence cannot be guaranteed. In [41], a distributed finite-time homogeneous controller was proposed to achieve the aim of velocity-free. However, the finite-time convergence analysis is unclear when the system is subject to various disturbances and actuator faults. To address this challenge, a model-free velocity observer was developed in [42] to realize the velocity-free attitude control, but its estimation speed is relatively slow. Notably, the precise reconstruction of angular velocity is important for the system stability, and this is also one of our aims.

In reality, the actuator faults and input saturation should be considered, otherwise it could cause mechanical failure and unpredictable consequences. Current results on how to solve the input saturation mainly include: i) the small-gain approach is used to reduce the input amplitude [43]; ii) the auxiliary system or observer technique is constructed to compensate for the saturation difference [44]–[46]; and iii) the continuous function is adopted to approximate the discontinuous signal [47]. However, there are some problems that needed to be improved, such as free singularity, fast saturation elimination, and compensation-error ability. For another problem, many FTCs have been developed to guarantee the safety of the system. In [48], an active FTC-based observer was developed to tackle the actuator faults, while the fault-tolerant ability depends on the accuracy of the fault estimation. As a key component of the active FTC, the fault detection and isolation (FDI) could increase the complexity of the FTC. To solve the above problems, some passive FTCs were proposed in [22], [49]–[51]. By combining the benefits of FLS and DO, the parametric uncertainties and fault components were resolved [22], [49]. In [50], the *authors* proposed a finite-time FTC via the Lyapunov-Krasovskii function. Xiao *et al.* [51] designed a projection-based adaptive algorithm to overcome the actuator faults while ensuring the boundedness of the adaptive parameters. Compared with the active FTC, the passive FTC can address the actuator faults without any FDI process and is robust in solving a group of considered faults.

Although diverse results have been obtained, solving all the aforesaid factors simultaneously brings major challenges. This study develops an observer-based adaptive fuzzy finite-time attitude controller for quadrotor UAVs with unavailable angular velocity, external disturbances, parametric uncertainties, actuator faults, and input saturation, which can realize free singularity, satisfactory robustness, chattering avoidance, fault tolerance, and saturation elimination. First, an AFTNNO is proposed to estimate the accurate information of angular velocity. Then, an adaptive FLS-based NFTSMC is designed to improve the system robustness. Besides, an auxiliary system is constructed to solve the input saturation. By comparison, the main contributions of this study are summarized as

1) In contrast to the previous state observers in [20], [23], [38], [41], the designed adaptive finite-time NN observer (AFTNNO) can estimate the information of angular velocity without the accurate knowledge of the system dynamics. Meanwhile, the AFTNNO not only keeps the basic property of the controller with the full-state measurable compared with the state observer in [23], but also realizes the finite-time convergence rather than the exponential convergence in [38]–[40] and provides a faster convergence speed than the state observer in [42]. These infer the AFTNNO can achieve better estimation performance.
2) In comparison with the conventional fuzzy SMCs in [3], [18], [22] and fuzzy logic controllers in [15]–[17], [19]–[21], the designed adaptive FLS-based NFTSMC strategy not only has a simpler fuzzy structure, fewer logic rules and free singularity, but also updates fuzzy gain automatically, achieves the finite-time stability and improves the convergence speed, which helps overcome the undesired chattering and enhance the steady-state performance. When the tracking errors are close to the sliding mode surface, the fuzzy switching control part is removed to decrease the unnecessary energy loss. Furthermore, compared with the

current works in [10], [13], [17], [22], [26], [35], where the lumped disturbance $\boldsymbol{D}$ and its derivative $\dot{\boldsymbol{D}}$ are both bounded [17], [22], [26], $\dot{\boldsymbol{D}}$ changes slowly (i.e., $\dot{\boldsymbol{D}} = \boldsymbol{0}$) [13], or the bound of $\boldsymbol{D}$ needs to be known [10], [35], this work just requires $\boldsymbol{D}$ to be bounded. These could release the application limitation and possess higher adaptability.

3) Compared with the previous approaches in [44], [45], [47] to tackle the input saturation, the designed auxiliary system not only guarantees the finite-time stability without the boundedness of the saturation region, but also overcomes the singularity issue and the saturation-compensation error, which are beneficial to improve the saturation rejection capability. Extensive comparative simulations and real-time experiments are executed to demonstrate the effectiveness and advantages of the developed control strategy.

The rest of this paper is described as follows: Section II describes some preliminaries. Section III gives the controller development and the stability analysis. Section IV performs comparative simulations and experiments. In Section V, conclusive statements are given.

Notations: $\boldsymbol{I}_{p\times p}$, $\boldsymbol{0}_{p\times p}$, and $\mathrm{tr}(\bullet)$ are the $p\times p$ identity matrix, the $p\times p$ zero matrix, and the matrix's trace, respectively. $\lambda_{\min}(\bullet)$ and $\lambda_{\max}(\bullet)$ stand for the minimum and maximum singular values of a matrix. For any vector $\boldsymbol{y}\in\mathbb{R}^m$ and a scalar $b>1$, $\mathrm{sign}(\boldsymbol{y})^b$ is defined as $\mathrm{sign}(\boldsymbol{y})^b = \left[|y_1|^b\mathrm{sign}(y_1);\ldots;|y_m|^b\mathrm{sign}(y_m)\right]$, which can be proved that $\frac{d}{dt}(\mathrm{sign}(\boldsymbol{y})^b) = b|\boldsymbol{y}|^{b-1}\dot{\boldsymbol{y}}$. The subscript $\times$ is a transformation of a vector $\boldsymbol{z}=[z_1;z_2;z_3]$ to skew-symmetric matrix, which can be written by $[\boldsymbol{z}]_\times = [0,-z_3,z_2;z_3,0,-z_1;-z_2,z_1,0]$.

II. Preliminaries and Problem Formulation

A. System Description

The physical structure of the quadrotor UAV is vividly shown in Fig. 1, where the coordinate frames $\mathcal{A}$ and $\mathcal{B}$ stand for the earth-fixed and body-fixed frames, respectively. The relation of attitude angle $\boldsymbol{\Theta}=[\phi;\theta;\varphi]$ and angular velocity $\boldsymbol{\Omega}=[p_b;q_b;r_b]$ is given by

$$\boldsymbol{\Omega} = \boldsymbol{R}_s(\boldsymbol{\Theta})\dot{\boldsymbol{\Theta}} = \begin{bmatrix} 1 & S_\phi T_\theta & C_\phi T_\theta \\ 0 & C_\phi & -S_\phi \\ 0 & S_\phi/C_\theta & C_\phi/C_\theta \end{bmatrix}\dot{\boldsymbol{\Theta}} \tag{1}$$

where $S_i \triangleq \sin(i)$, $C_i \triangleq \cos(i)$, and $T_i \triangleq \tan(i)$, $i=\phi,\theta,\varphi$. Notice that the Euler angles ϕ and θ are limited to $(-\frac{\pi}{2},\frac{\pi}{2})$, which is physically meaningful to ensure the quadrotor UAV never be overturned and to prevent the singular issue in the Euler angle propagation equations [1], [13], [20].

The quadrotor attitude dynamics can be modeled via Euler-Lagrangian methodology, as [4], [9]:

$$\boldsymbol{J}\dot{\boldsymbol{\Omega}} = -[\boldsymbol{\Omega}]_\times\boldsymbol{J}\boldsymbol{\Omega} + \boldsymbol{u} + \boldsymbol{d} \tag{2}$$

where $\boldsymbol{u}=[u_1;u_2;u_3]$ and $\boldsymbol{J}=\mathrm{diag}\{J_x,J_y,J_z\}$ are the control input and inertial matrix, respectively; $\boldsymbol{d}=[d_1;d_2;d_3]$ denotes the disturbance disturbance factor.

Assumption 1 [21]: With the consideration of the structural flexibility and load changes, the inertial matrix $\boldsymbol{J}$ can be described as $\boldsymbol{J}=\boldsymbol{J}_0+\boldsymbol{J}_\triangle$, where $\boldsymbol{J}_0=\left[J_{0,x};J_{0,y};J_{0,z}\right]$

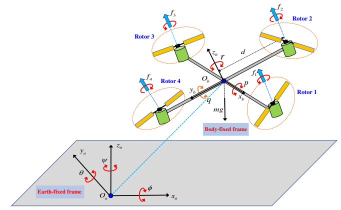

Fig. 1. Physical structure of the quadrotor UAV

and $\boldsymbol{J}_\triangle=\left[J_{\triangle,x};J_{\triangle,y};J_{\triangle,z}\right]$ denote the ideal part and uncertain part of $\boldsymbol{J}$, respectively, which is reasonable to assume $\|\boldsymbol{J}_\triangle\|\le\bar{J}$ with $\bar{J}>0$ denoting an unknown scalar.

Assumption 2 [21]: The external disturbance $\boldsymbol{d}$ is unknown but bounded by an unknown constant $\bar{d}>0$, i.e., $\|\boldsymbol{d}\|\le\bar{d}$.

B. Analysis of Actuator Faults and Input Saturation

The control input with actuator faults and input saturation can be generally expressed by [22], [44]:

$$\boldsymbol{u} = \boldsymbol{E}\mathrm{sat}(\boldsymbol{u}_o) + \boldsymbol{u}_f \tag{3}$$

where $\boldsymbol{u}_o=[u_{o,1};u_{o,2};u_{o,3}]$ is the designed control input. The additive fault $\boldsymbol{u}_f=[u_{f,1};u_{f,2};u_{f,3}]$ represents the uncontrollable portion of the control input that is unmeasurable and time-varying. In a real quadrotor UAV system, $\boldsymbol{u}_f$ means the external input, such as wind disturbances, the dampings from various frictions, or the force bias induced by the electric regulator errors of the motors. $\boldsymbol{E}=\mathrm{diag}\{e_1,e_2,e_3\}$ is the actuation effectiveness matrix. This study considers the following types of actuator faults:

1) *Type 1:* If $e_i=1$ and $u_{f,i}=0$, it means that the ith actuator is healthy.
2) *Type 2:* If $e_i=1$ and $u_{f,i}\neq 0$, it means that the ith actuator is additive fault.
3) *Type 3:* If $e_i\in(0,1)$ and $u_{f,i}=0$, it means that the ith actuator is partial effectiveness.
4) *Type 4:* If $e_i\in(0,1)$ and $u_{f,i}\neq 0$, it means that the ith actuator is partial effectiveness and additive failure.

Assumption 3 [32], [44]: The parameters $u_{f,i}$ and e_i satisfy the conditions such that $|u_{f,i}|<\infty$ and $0<e_i\le 1$.

The actual input $\mathrm{sat}(u_{o,i}(t))$ can be characterized by

$$\mathrm{sat}(u_{o,i}(t)) = \begin{cases} \underline{u}_i, & u_{o,i}(t)<\underline{u}_i \\ g_{r,i}(u_{o,i}(t)), & \underline{u}_i\le u_{o,i}(t)\le 0 \\ g_{l,i}(u_{o,i}(t)), & 0<u_{o,i}(t)\le\bar{u}_i \\ \bar{u}_i, & u_{0,i}(t)>\bar{u}_i \end{cases} \tag{4}$$

where $\underline{u}_i<0$ and $\bar{u}_i>0$ are the known lower and upper bounds on $u_{o,i}(t)$, and $g_{r,i}(\cdot)$ and $g_{l,i}(\cdot)$ are unknown nonlinearities. Thus, the attitude model of the quadrotor UAV can be expressed by

$$\boldsymbol{N}_1(\boldsymbol{\Theta})\ddot{\boldsymbol{\Theta}} + \boldsymbol{N}_2(\boldsymbol{\Theta},\dot{\boldsymbol{\Theta}})\dot{\boldsymbol{\Theta}} = \boldsymbol{R}_t^{\mathrm{T}}\mathrm{sat}(\boldsymbol{u}_0) + \boldsymbol{D} \tag{5}$$

where $\boldsymbol{R}_t$ is the inverse matrix of $\boldsymbol{R}_s$ (i.e., $\boldsymbol{R}_t=\boldsymbol{R}_s^{-1}$), $\boldsymbol{N}_1=\boldsymbol{R}_t^{\mathrm{T}}\boldsymbol{J}_0\boldsymbol{R}_t$, $\boldsymbol{N}_2=\boldsymbol{R}_t^{\mathrm{T}}\boldsymbol{J}_0\dot{\boldsymbol{R}}_t-\boldsymbol{R}_t^{\mathrm{T}}\left[\boldsymbol{J}_0\boldsymbol{R}_t\dot{\boldsymbol{\Theta}}\right]_\times\boldsymbol{R}_t$ and $\boldsymbol{D}=\boldsymbol{R}_t^{\mathrm{T}}\big(\boldsymbol{d}+\boldsymbol{J}_\triangle\boldsymbol{R}_t+\boldsymbol{J}_\triangle\dot{\boldsymbol{R}}_t-\left[\boldsymbol{J}_\triangle\boldsymbol{R}_t\dot{\boldsymbol{\Theta}}\right]_\times\boldsymbol{R}_t+(\boldsymbol{E}-\boldsymbol{I}_{3\times3})\mathrm{sat}(\boldsymbol{u}_0)+\boldsymbol{u}_f\big)$. It is worth emphasizing that since the Euler angle θ is constrained to $-\frac{\pi}{2}<\theta<\frac{\pi}{2}$, $\boldsymbol{R}_t$ is nonsingular. On the basis of this, each elements of $\boldsymbol{N}_1$ and $\boldsymbol{N}_2$ are respectively written by

$$\boldsymbol{N}_1 = \begin{bmatrix} m_{11} & 0 & m_{13} \\ 0 & m_{22} & m_{23} \\ m_{13} & m_{23} & m_{33} \end{bmatrix}, \ \boldsymbol{N}_2 = \begin{bmatrix} n_{11} & n_{12} & n_{13} \\ n_{21} & n_{22} & n_{23} \\ n_{31} & n_{32} & n_{33} \end{bmatrix}$$

where $m_{11} = J_{0,x}$, $m_{13} = -J_{0,x}S_\theta$, $m_{22} = J_{0,y}C_\phi^2 + J_{0,z}S_\phi^2$, $m_{23} = (J_{0,y} - J_{0,z})C_\phi S_\phi C_\theta$, and $m_{33} = J_{0,x}S_\theta^2 + J_{0,y}S_\phi^2 C_\theta^2 + J_{0,z}C_\phi^2 C_\theta^2$; $n_{11} = 0$, $n_{12} = (J_{0,y} - J_{0,z})\big(\dot{\theta} C_\phi S_\phi + \dot{\varphi} S_\phi^2 C_\theta\big) - J_{0,x}\dot{\varphi} C_\theta + (J_{0,z} - J_{0,y})\dot{\varphi} C_\phi^2 C_\theta$, $n_{13} = (J_{0,z} - J_{0,y})\dot{\varphi} C_\phi^2 S_\phi C_\theta^2$, $n_{21} = -(J_{0,y} - J_{0,z})\big(\dot{\theta} C_\phi S_\phi + \dot{\varphi} S_\phi^2 C_\theta\big) + J_{0,x}\dot{\varphi} C_\theta - (J_{0,z} - J_{0,y})\dot{\varphi} C_\phi^2 C_\theta$, $n_{22} = (J_{0,z} - J_{0,y})\dot{\phi} C_\phi S_\phi$, $n_{23} = -J_{0,x}\dot{\varphi} S_\theta C_\theta + J_{0,y}\dot{\varphi} S_\phi^2 C_\theta S_\theta + J_{0,z}\dot{\varphi} C_\phi^2 S_\theta C_\theta$, $n_{31} = (J_{0,y} - J_{0,z})\dot{\varphi} C_\theta^2 S_\phi C_\phi - J_{0,x}\dot{\theta} C_\theta$, $n_{32} = (J_{0,z} - J_{0,y})\big(\dot{\theta} C_\phi S_\phi S_\theta + \dot{\phi} S_\phi^2 C_\theta\big) + J_{0,x}\dot{\varphi} S_\theta C_\theta - (J_{0,z} - J_{0,y})\dot{\phi} C_\phi^2 C_\theta - J_{0,y}\dot{\varphi} S_\phi S_\theta C_\theta - J_{0,z}\dot{\varphi} C_\phi S_\theta C_\theta$, and $n_{33} = (J_{0,y} - J_{0,z})\dot{\phi} C_\phi S_\phi C_\theta^2 - J_{0,y}\dot{\theta} S_\phi^2 C_\theta S_\theta + J_{0,x}\dot{\theta} C_\theta S_\theta - J_{0,z}\dot{\theta} C_\phi^2 C_\theta S_\theta$. Thus, it can be concluded that $\boldsymbol{N}_1^{-1}$ and $\boldsymbol{N}_2^{-1}$ are nonsingular.

Assumption 4: The lumped disturbance $\boldsymbol{D}$ satisfies $\|\boldsymbol{D}\| \le \bar{D}$, where $\bar{D} > 0$ is an unknown scalar.

Remark 1: In this article, the problems of the external disturbances, uncertain parameters, actuator faults, input saturation, and unmeasurable angular velocity are considered simultaneously in the attitude dynamics. Because this could lead to the complexity of the controller development and model establishment, most prior studies in [7]–[10], [12] only considered part of the aforesaid issues. Moreover, in contrast to the previous study in [6], the pitch angle and roll angle are not assumed to vary near zero and be relatively small. Therefore, the considered situations are more realistic.

Remark 2: For Assumptions 1–4, it is necessary to make further discussions: (i) The uncertain inertia matrix is usually caused by the deployment of sensors, the structural flexibility and the change in payloads, Assumption 1 is thus general [21]. (ii) Since the external disturbances like wind gusts, aerodynamic friction and gyroscopic effect are constantly changing and have the limited energy influence, the external disturbances acting on the quadrotor UAV can thus be regarded as unknown time-varying yet bounded commands. (iii) In fact, insufficient battery power would lead to the degradation of the actuator effectiveness, and due to the limited energy and the avoidance of infinite control gain, Assumption 3 is standard to describe the actuator faults [32], [44]. (iv) Since the lumped disturbance $\boldsymbol{D}$ contains the external disturbance, uncertain inertia, and actuator faults, it is reasonable to assume that $\boldsymbol{D}$ is bounded. Besides, in contrast with [10], [13], [17], [22], [26], [35], where the lumped disturbance $\boldsymbol{D}$ and its derivative $\dot{\boldsymbol{D}}$ are both bounded [17], [22], [26], $\dot{\boldsymbol{D}}$ changes slowly (i.e., $\dot{\boldsymbol{D}} = \boldsymbol{0}$) [13], or the bound of $\boldsymbol{D}$ is known [10], [35], this study only requires that $\boldsymbol{d}$ is bounded by an unknown scalar. Thus, Assumption 4 removes the application restriction.

C. RBFNN Approximation

Any unknown nonlinear function $\mathcal{F}(\boldsymbol{Z}) : \mathbb{R}^w \to \mathbb{R}$ can be approximated by the following RBFNN:

$$\mathcal{F}(\boldsymbol{Z}) = \boldsymbol{W}^{*\mathrm{T}}\boldsymbol{h}(\boldsymbol{Z}) + \delta(\boldsymbol{Z}) \tag{6}$$

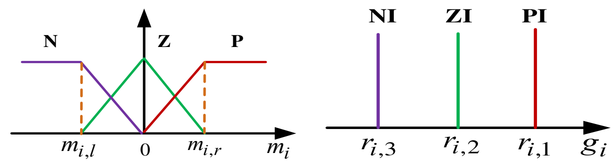

(a) Input fuzzy sets for $\boldsymbol{m}$ (b) Output fuzzy sets for $\boldsymbol{r}_i$

Fig. 2. Illustration of Membership functions.

where $\boldsymbol{Z} \in \Omega_Z \subset \mathbb{R}^w$ is the RBFNN's input, $\delta(\boldsymbol{Z})$ is the approximation error and holds $\|\delta(\boldsymbol{Z})\| \le \bar{\eta}$ with $\bar{\eta}$ being a positive scalar, and $\boldsymbol{h}(\boldsymbol{Z}) \in \mathbb{R}^p$ can be written by [12]

$$h_i(\boldsymbol{Z}) = \exp\left[\frac{(\boldsymbol{Z} - \boldsymbol{C}_i)^{\mathrm{T}}(\boldsymbol{Z} - \boldsymbol{C}_i)}{\kappa_i^2}\right], \ i = 1, \cdots, p \tag{7}$$

where $\boldsymbol{C}_i \in \mathbb{R}^w$ and $\kappa_i > 0$ represent the center of the receptive field and the width of $h_i(\boldsymbol{Z})$, respectively. In addition, $\boldsymbol{W}^* \in \mathbb{R}^p$ expresses the ideal weight vector calculated by [14]

$$\boldsymbol{W}^* = \arg\min_{\hat{\boldsymbol{W}}^*}\left\{\sup_{Z\in\Omega_Z}\left|\mathcal{F}(\boldsymbol{Z}) - \hat{\boldsymbol{W}}^{*\mathrm{T}}\boldsymbol{h}(\boldsymbol{Z})\right|\right\}. \tag{8}$$

where $\hat{\boldsymbol{W}}^* \in \mathbb{R}^p$ is the estimation of $\boldsymbol{W}^*$, $\bar{W}$ is the upper bound of $\|\boldsymbol{W}^*\|$, $p > 1$ is the the node number of RBFNN. Note that the ideal network weight $\boldsymbol{W}^*$ is unknown and used only for analysis objectives, and it needs to be estimated in the design procedure.

D. FLS Design

The fuzzy inference engine uses a set of *IF-THEN* rules to perform a mapping from the input $\boldsymbol{m} = [m_1, \ldots, m_n]^{\mathrm{T}} \in \mathbb{R}^n$ to the output $\boldsymbol{g} = [g_1, \ldots, g_n]^{\mathrm{T}} \in \mathbb{R}^n$, where m_i and g_i are described by

- m_i [antecedent proposition]: P (positive), N (negative), Z (zero);
- g_i [consequent proposition]: PI (positive influence), NI (negative influence), ZI (zero influence).

In this study, the fuzzy linguistic rule bases are given by

- *Rule 1*: If m_i belongs to P, then g_i belongs to PI.
- *Rule 2*: If m_i belongs to Z, then g_i belongs to ZI.
- *Rule 3*: If m_i belongs to N, then g_i belongs to NI.

The membership functions of m_i and g_i are shown in Fig. 2, and the choice of $m_{i,r}$ and $m_{i,l}$ is based on the performance demands. From the perspective of simple calculation and intuitive credibility, the singleton fuzzification with triangular membership function and center of gravity defuzzification scheme is employed. As a result, one obtains

$$g_i = \frac{\sum_{j=1}^{3} v_{i,j} r_{i,j}}{\sum_{j=1}^{3} v_{i,j}} = \frac{(v_{i,1}r_{i,1} + v_{i,2}r_{i,2} + v_{i,3}r_{i,3})}{(v_{i,1} + v_{i,2} + v_{i,3})} \tag{9}$$

where $v_{i,j} \in [0, 1]$ is the firing strength of *Rule* j. The fuzzy gains $r_{i,1}$, $r_{i,2}$ and $r_{i,3}$ need to be chosen suitably, and $r_{i,1} = r_{a,i}$, $r_{i,2} = 0$ and $r_{i,3} = -r_{a,i}$ are the centers of PI, ZI, and NI, respectively; the relation $v_{i,1} + v_{i,2} + v_{i,3} = 1$ is true since it meets the special situation of triangular membership function. Next, this study will analyze only four possible situations:

- *Situation 1*: Only *Rule 1* satisfies (i.e., $v_{i,1}=1$, $v_{i,2}=0$ and $v_{i,3}=0$), one gets $g_i=r_{a,i}$.
- *Situation 2*: Both *Rules 1* and *2* satisfy (i.e., $0<v_{i,1}<1$, $0<v_{i,2}<1$ and $v_{i,3}=0$), one gets $g_i=v_{i,1}r_{i,1}=v_{i,1}r_{a,i}$.
- *Situation 3*: Both *Rules 2* and *3* satisfy (i.e., $v_{i,1}=0$, $0<v_{i,2}<1$ and $0<v_{i,3}<1$), one gets $g_i=v_{i,3}r_{i,3}=-v_{i,3}r_{a,i}$.
- *Situation 4*: Only *Rule 3* satisfies (i.e., $v_{i,1}=0$, $v_{i,2}=0$ and $v_{i,3}=1$), one gets $g_i=-r_{a,i}$.

Thus, one can get a conclusion $(v_{i,1}-v_{i,3})r_{a,i}=|(v_{i,1}-v_{i,3})r_{a,i}|\geq 0$, and the following result holds

$$g_i=(v_{i,1}-v_{i,3})r_{a,i}. \tag{10}$$

Further, the final output of the designed FLS can be written as $\boldsymbol{g}=(\boldsymbol{v}_1-\boldsymbol{v}_3)\boldsymbol{r}_a$, where $\boldsymbol{r}_a=[r_{a,1},\ldots,r_{a,n}]^{\mathrm{T}}\in\mathbb{R}^n$, $\boldsymbol{v}_1=\mathrm{diag}\{v_{1,1},\ldots,v_{n,1}\}\in\mathbb{R}^{n\times n}$, and $\boldsymbol{v}_3=\mathrm{diag}\{v_{1,3},\ldots,v_{n,3}\}\in\mathbb{R}^{n\times n}$.

Remark 3: To realize low-computation fuzzy approximation, the number of fuzzy rules is unexpected to be large. In this study, the total number of fuzzy rules is less than in previous studies on the attitude control of the quadrotor UAV [3], [15], [17]. Particularly, this study performs comparative simulations and experiments to verify that even though the number of fuzzy rules is reduced, good control performance can still be achieved.

Lemma 1 [36]: For a scalar $\beta>0$ and any two matrices $\boldsymbol{P}$ and $\boldsymbol{Q}$ with appropriate dimensions, it follows that $2\boldsymbol{P}^{\mathrm{T}}\boldsymbol{Q}\leq\beta\boldsymbol{P}^{\mathrm{T}}\boldsymbol{P}+\beta^{-1}\boldsymbol{Q}^{\mathrm{T}}\boldsymbol{Q}$.

Lemma 2 [4]: For a scalar $h\in(0,1]$ and any variable x_i, the following inequality holds:

$$\left(\sum\nolimits_{i=1}^{n}|x_i|\right)^h\leq\sum\nolimits_{i=1}^{n}|x_i|^h\leq n^{1-h}\left(\sum\nolimits_{i=1}^{n}|x_i|\right)^h. \tag{11}$$

Lemma 3 [32]: For the nonlinear system $\dot{x}=f(x)$, $f(0)=0$, $x\in\mathbb{R}^n$, suppose there exist a Lyapunov function $V(x)$ and some scalars $0<\eta<\infty$, $\pi_1>0$, $\pi_2>0$ and $0<\pi_3<1$ such that $\dot{V}(x)\leq-\pi_1V(x)-\pi_2V^{\pi_3}(x)+\eta$. Then, the system is fast practically finite-time stable and the function $V(x)$ converges to the following bounded region, as

$$\lim_{t\to T}V(x)\leq\min\left\{\frac{\eta}{(1-\epsilon)\pi_1},\left(\frac{\eta}{(1-\epsilon)\pi_2}\right)^{1/\pi_3}\right\} \tag{12}$$

where $\epsilon\in(0,1)$, and the convergence time T is bounded by

$$T\leq\max\left\{t_0+\frac{1}{\epsilon\pi_1(1-\pi_3)}\ln\frac{\epsilon\pi_1V^{1-\pi_3}(t_0)+\pi_2}{\pi_2},\right.$$
$$\left.t_0+\frac{1}{\pi_1(1-\pi_3)}\ln\frac{\pi_1V^{1-\pi_3}(t_0)+\epsilon\pi_2}{\epsilon\pi_2}\right\} \tag{13}$$

where t_0 is the initial time.

Lemma 4 [31]: For a Gauss' hypergeometric function:

$$\Lambda(\chi_1,\chi_2,\chi_3,\chi_4)=\sum\nolimits_{k=0}^{\infty}\frac{(\chi_1)_k(\chi_2)_k}{(\chi_3)_kk!}\chi_4^k \tag{14}$$

if χ_1, χ_2, and χ_3 are positive constants and satisfy the condition $\chi_3-\chi_2-\chi_1>0$, the function $\Lambda(\cdot)$ is convergent within the definition domain $\chi_4<0$.

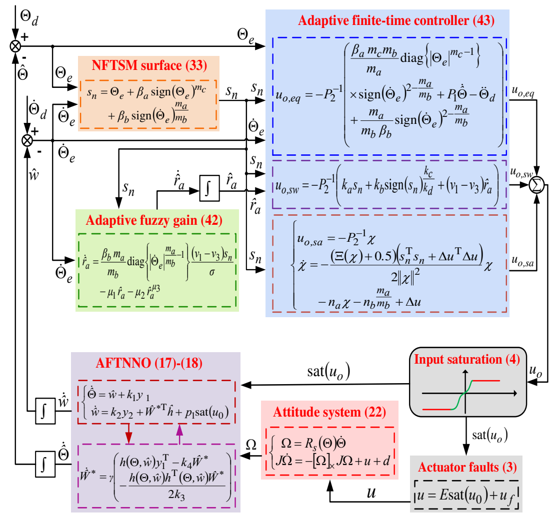

Fig. 3. Block diagram of the presented control framework.

Lemma 5 [24]: For any variable z, a constant ϵ_1, $0<p<1$, and $0<q=\frac{q_1}{q_2}<1$, where q_1 and q_2 are positive odd integers, the following inequality is valid:

$$-z(z+\epsilon_1)^q\leq-\frac{1-p}{1+q}z^{1+q}+\frac{\epsilon_2}{1+q} \tag{15}$$

where $\epsilon_2=\epsilon_1^{1+q}+\left(\frac{\epsilon_1}{1-(1-p)^{1/(1+q)}}\right)^{1+q}+\left(\frac{\epsilon_1(1-p)^{1/(1+q)}}{1-(1-p)^{1/(1+q)}}\right)^{1+q}$.

III. Controller Design and Stability Analysis

Firstly, an AFTNNO is proposed to estimate the angular velocity. Then, this study designs an observer-based adaptive fuzzy finite-time attitude controller to deal with various disturbances. Finally, the stability analysis is given. For the convenience of the reader, the overall block diagram for the attitude control system is vividly shown in Fig. 3.

A. AFTNNO Design

First, by letting a new state variable as $\boldsymbol{w}=\dot{\boldsymbol{\Theta}}$, one gets

$$\begin{cases}\dot{\boldsymbol{\Theta}}=\boldsymbol{w}\\ \dot{\boldsymbol{w}}=\boldsymbol{f}(\boldsymbol{\Theta},\boldsymbol{w})+\boldsymbol{p}_1\mathrm{sat}(\boldsymbol{u}_0)+\boldsymbol{p}_2(\boldsymbol{u}_f+\boldsymbol{d})\end{cases} \tag{16}$$

where $\boldsymbol{f}=-\boldsymbol{R}_t\boldsymbol{J}_0^{-1}\left[\boldsymbol{R}_s\boldsymbol{w}\right]_\times\boldsymbol{J}\boldsymbol{R}_s\boldsymbol{w}-\boldsymbol{R}_t\boldsymbol{J}_0^{-1}\boldsymbol{J}_\Delta(\dot{\boldsymbol{R}}_s\boldsymbol{w}+\boldsymbol{R}_s\dot{\boldsymbol{w}})+\dot{\boldsymbol{R}}_t\boldsymbol{R}_s\boldsymbol{w}$, $\boldsymbol{p}_1=\boldsymbol{R}_t\boldsymbol{J}_0^{-1}$, and $\boldsymbol{p}_2=\boldsymbol{R}_t\boldsymbol{J}_0^{-1}$.

Then, an AFTNNO is designed as

$$\begin{cases}\dot{\hat{\boldsymbol{\Theta}}}=\hat{\boldsymbol{w}}+k_1\boldsymbol{y}_1\\ \dot{\hat{\boldsymbol{w}}}=k_2\boldsymbol{y}_2+\hat{\boldsymbol{W}}^{*\mathrm{T}}\hat{\boldsymbol{h}}(\hat{\boldsymbol{\Theta}},\hat{\boldsymbol{w}})+\boldsymbol{p}_1\mathrm{sat}(\boldsymbol{u}_0)\end{cases} \tag{17}$$

where $\hat{\boldsymbol{\Theta}}=\left[\hat{\phi};\hat{\theta};\hat{\varphi}\right]$, $\hat{\boldsymbol{w}}=\left[\dot{\hat{\phi}};\dot{\hat{\theta}};\dot{\hat{\varphi}}\right]$ and $\hat{\boldsymbol{W}}^*$ stand for the estimations of $\boldsymbol{\Theta}$, $\boldsymbol{w}$ and $\boldsymbol{W}^*$, respectively; $k_1>0$ and $k_2>0$ are design parameters; $\boldsymbol{y}_1=\mathrm{sign}^{\frac{3l-2}{l}}(\tilde{\boldsymbol{\Theta}})+k_3\tilde{\boldsymbol{\Theta}}$, $\boldsymbol{y}_2=k_3\boldsymbol{y}_1+\frac{3l-2}{l}\left(\mathrm{sign}^{\frac{5l-4}{l}}(\tilde{\boldsymbol{\Theta}})+k_3\mathrm{sign}^{\frac{3l-2}{l}}(\tilde{\boldsymbol{\Theta}})\right)$, $\tilde{\boldsymbol{\Theta}}=\boldsymbol{\Theta}-\hat{\boldsymbol{\Theta}}$, and $k_3>0$. Here should satisfy $\frac{4}{5}<l<1$ and $2l-1=\frac{l_1}{l_2}$, where l_1 and l_2 are positive odd integers. In this study, $\hat{\boldsymbol{W}}^*$ can be adjusted by

$$\dot{\hat{\boldsymbol{W}}}^*=\boldsymbol{\Upsilon}\left(\hat{\boldsymbol{h}}\boldsymbol{y}_1^{\mathrm{T}}-k_4\hat{\boldsymbol{W}}^*-\frac{\hat{\boldsymbol{h}}\hat{\boldsymbol{h}}^{\mathrm{T}}\hat{\boldsymbol{W}}^*}{2k_3}\right) \tag{18}$$

where $\boldsymbol{\Upsilon} \in \mathbb{R}^{3\times 3}$ is a positive-definite matrix and $k_4 > 0$. By denoting $\tilde{\boldsymbol{w}} = \boldsymbol{w} - \hat{\boldsymbol{w}}$, $\tilde{\boldsymbol{W}}^* = \boldsymbol{W}^* - \hat{\boldsymbol{W}}^*$ and $\tilde{\boldsymbol{h}} = \boldsymbol{h}(\boldsymbol{\Theta}, \boldsymbol{w}) - \hat{\boldsymbol{h}}(\hat{\boldsymbol{\Theta}}, \hat{\boldsymbol{w}})$, it follows that

$$\begin{cases} \dot{\tilde{\boldsymbol{\Theta}}} = \tilde{\boldsymbol{w}} - k_1 \boldsymbol{y}_1 \\ \dot{\tilde{\boldsymbol{w}}} = -k_2 \boldsymbol{y}_2 + \tilde{\boldsymbol{W}}^{*\mathrm{T}} \hat{\boldsymbol{h}} + \hat{\boldsymbol{W}}^{*\mathrm{T}} \tilde{\boldsymbol{h}} + \Xi \end{cases} \tag{19}$$

wherein $\Xi = \boldsymbol{f} + \boldsymbol{p}_2(\boldsymbol{u}_f + \boldsymbol{d})$. For simplicity, we denote a new estimation error as $\boldsymbol{\xi} = \left[\boldsymbol{\xi}_1^{\mathrm{T}}; \boldsymbol{\xi}_2^{\mathrm{T}}\right] = \left[\boldsymbol{y}_1^{\mathrm{T}}; \tilde{\boldsymbol{w}}^{\mathrm{T}}\right]$. Then, the time derivative of $\boldsymbol{\xi}$ along (16)–(19) is given by

$$\dot{\boldsymbol{\xi}} = \left(a\boldsymbol{A}_1 + k_3\right)\boldsymbol{A}_2 \boldsymbol{\xi} + \boldsymbol{A}_3\left(\tilde{\boldsymbol{W}}^{*\mathrm{T}} \hat{\boldsymbol{h}} + \hat{\boldsymbol{W}}^{*\mathrm{T}} \tilde{\boldsymbol{h}} + \boldsymbol{\Xi}\right) \tag{20}$$

where $\boldsymbol{A}_1 = \left[\mathrm{diag}\left\{|\tilde{\boldsymbol{\Theta}}|^{\frac{2l-2}{l}}\right\}, \boldsymbol{0}_{3\times 3}; \boldsymbol{0}_{3\times 3}, \mathrm{diag}\left\{|\tilde{\boldsymbol{\Theta}}|^{\frac{2l-2}{l}}\right\}\right] \in \mathbb{R}^{6\times 6}$, $\boldsymbol{A}_2 = \left[-k_1 \boldsymbol{I}_{3\times 3}, \boldsymbol{I}_{3\times 3}; -k_2 \boldsymbol{I}_{3\times 3}, \boldsymbol{0}_{3\times 3}\right] \in \mathbb{R}^{6\times 6}$, $\boldsymbol{A}_3 = \left[\boldsymbol{0}_{3\times 3}; \boldsymbol{I}_{3\times 3}\right] \in \mathbb{R}^{6\times 3}$ and $a = \frac{3l-2}{l}$. Denote two matrices as $\boldsymbol{B} = \left[\boldsymbol{I}_{3\times 3}, \boldsymbol{0}_{3\times 3}\right] \in \mathbb{R}^{6\times 6}$, and $\boldsymbol{E} = \boldsymbol{B}^{\mathrm{T}} - \boldsymbol{C}\boldsymbol{A}_3$ with $\boldsymbol{C} \in \mathbb{R}^{3\times 6}$ being a positive-definite matrix.

Theorem 1: For the attitude system (16) and the presented AFTNNO (17) and (18), the estimation errors $\tilde{\boldsymbol{\Theta}}$, $\tilde{\boldsymbol{w}}$ and $\tilde{\boldsymbol{W}}^*$ converge to the bounded regions in finite time, if the positive-definite matrix $\boldsymbol{C}$ holds the linear matrix inequalities, as:

$$\boldsymbol{C}\boldsymbol{A}_2 + \boldsymbol{A}_2^{\mathrm{T}}\boldsymbol{C} < -\boldsymbol{K}_1 \tag{21a}$$

$$\boldsymbol{C}\boldsymbol{A}_2 + \boldsymbol{A}_2^{\mathrm{T}}\boldsymbol{C} + \boldsymbol{E}\boldsymbol{E}^{\mathrm{T}} < -\boldsymbol{K}_2 \tag{21b}$$

where $\boldsymbol{E} = \boldsymbol{B}^{\mathrm{T}} - \boldsymbol{C}\boldsymbol{A}_3$ with $\boldsymbol{C} \in \mathbb{R}^{3\times 6}$ being a positive-definite matrix, $\boldsymbol{A}_3 = \left[\boldsymbol{0}_{3\times 3}; \boldsymbol{I}_{3\times 3}\right] \in \mathbb{R}^{6\times 3}$, $\boldsymbol{A}_2 = \left[-k_1 \boldsymbol{I}_{3\times 3}, \boldsymbol{I}_{3\times 3}; -k_2 \boldsymbol{I}_{3\times 3}, \boldsymbol{0}_{3\times 3}\right] \in \mathbb{R}^{6\times 6}$, $\boldsymbol{B} = \left[\boldsymbol{I}_{3\times 3}, \boldsymbol{0}_{3\times 3}\right] \in \mathbb{R}^{6\times 6}$, $\boldsymbol{K}_1$ and $\boldsymbol{K}_2$ are arbitrary positive-definite matrices, k_1 and k_2 are positive constants, $k_3 > \frac{2\nu\lambda_{\max}^2(\boldsymbol{C}\boldsymbol{A}_3)}{k_3\lambda_{\min}(\boldsymbol{K}_2)}$ with $\nu_1 > 0$ being an arbitrary parameter, and $k_4 > \frac{\bar{h}^2}{k_3}$.

Proof: Construct the Lyapunov function as

$$V_1 = \boldsymbol{\xi}^{\mathrm{T}}\boldsymbol{C}\boldsymbol{\xi} + \mathrm{tr}\left\{\tilde{\boldsymbol{W}}^{*\mathrm{T}}\boldsymbol{\Upsilon}^{-1}\tilde{\boldsymbol{W}}^{*\mathrm{T}}\right\}. \tag{22}$$

Taking the derivative of (22) yields

$$\begin{aligned}\dot{V}_1 =& a\boldsymbol{\xi}^{\mathrm{T}}\boldsymbol{A}_1\left(\boldsymbol{C}\boldsymbol{A}_2 + \boldsymbol{A}^{\mathrm{T}}\boldsymbol{C}\right)\boldsymbol{\xi} + k_3\boldsymbol{\xi}^{\mathrm{T}}\left(\boldsymbol{C}\boldsymbol{A}_2 + \boldsymbol{A}^{\mathrm{T}}\boldsymbol{C}\right)\boldsymbol{\xi} \\ &+ 2\boldsymbol{\xi}\boldsymbol{C}\boldsymbol{A}_3\left[\tilde{\boldsymbol{W}}^{*\mathrm{T}}\hat{\boldsymbol{h}} + \boldsymbol{W}^{*\mathrm{T}}\boldsymbol{h} + \Xi\right] + 2k_4\mathrm{tr}\left\{\tilde{\boldsymbol{W}}^{*\mathrm{T}}\hat{\boldsymbol{W}}^*\right\} \\ &+ k_3^{-1}\mathrm{tr}\left\{\tilde{\boldsymbol{W}}^{*\mathrm{T}}\hat{\boldsymbol{h}}\hat{\boldsymbol{h}}^{\mathrm{T}}\hat{\boldsymbol{W}}^{*\mathrm{T}}\right\} - 2\mathrm{tr}\left\{\tilde{\boldsymbol{W}}^{*\mathrm{T}}\hat{\boldsymbol{h}}\boldsymbol{y}_1^{\mathrm{T}}\right\}. \end{aligned} \tag{23}$$

With consideration of Lemma 5, Assumptions 1–4, and $\|\boldsymbol{R}_t\| = \frac{1}{\cos(\theta)} \le \nu_2 < \infty$, it follows that $\|\boldsymbol{\Xi}\| \le \|\boldsymbol{f}\| + \|\boldsymbol{p}\|\|\boldsymbol{d}\| \le \bar{\delta} + \nu_2\|\boldsymbol{J}_0^{-1}\|\bar{D} \triangleq \mu_{\max}$ with $\mu_{\max}$ being an unknown positive scalar. Hence, (23) can be rewritten as

$$\begin{aligned}\dot{V}_1 \le& -a\tilde{\Theta}_{\max}^{\frac{2l-2}{l}}\boldsymbol{\xi}^{\mathrm{T}}\boldsymbol{K}_1\boldsymbol{\xi} + k_3\boldsymbol{\xi}^{\mathrm{T}}\left(\boldsymbol{C}\boldsymbol{A}_2 + \boldsymbol{A}^{\mathrm{T}}\boldsymbol{C}\right)\boldsymbol{\xi} \\ &+ 2\nu\boldsymbol{\xi}^{\mathrm{T}}\lambda_{\max}^2\left(\boldsymbol{C}\boldsymbol{A}_3\right)\boldsymbol{\xi} + 2\boldsymbol{\xi}\boldsymbol{C}\boldsymbol{A}_3\tilde{\boldsymbol{W}}^{*\mathrm{T}}\hat{\boldsymbol{h}} + \nu_1^{-1} \\ &\times \tilde{\boldsymbol{h}}^{\mathrm{T}}\boldsymbol{W}^*\boldsymbol{W}^{*\mathrm{T}}\tilde{\boldsymbol{h}} + \nu_1^{-1}\boldsymbol{\Xi}^{\mathrm{T}}\boldsymbol{\Xi} + 2k_4\mathrm{tr}\left\{\tilde{\boldsymbol{W}}^{*\mathrm{T}}\hat{\boldsymbol{W}}^*\right\} \\ &+ k_3^{-1}\mathrm{tr}\left\{\tilde{\boldsymbol{W}}^{*\mathrm{T}}\hat{\boldsymbol{h}}\hat{\boldsymbol{h}}^{\mathrm{T}}\hat{\boldsymbol{W}}^{*\mathrm{T}}\right\} - 2\mathrm{tr}\left\{\tilde{\boldsymbol{W}}^{*\mathrm{T}}\hat{\boldsymbol{h}}\boldsymbol{y}_1^{\mathrm{T}}\right\} \\ \le& -a\tilde{\Theta}_{\max}^{\frac{2l-2}{l}}\boldsymbol{\xi}^{\mathrm{T}}\boldsymbol{K}_1\boldsymbol{\xi} + k_3\boldsymbol{\xi}^{\mathrm{T}}\left(\boldsymbol{C}\boldsymbol{A}_2 + \boldsymbol{A}^{\mathrm{T}}\boldsymbol{C}\right)\boldsymbol{\xi} \\ &+ 2\boldsymbol{\xi}\boldsymbol{C}\boldsymbol{A}_3\tilde{\boldsymbol{W}}^{*\mathrm{T}}\hat{\boldsymbol{h}} + 2\nu\boldsymbol{\xi}^{\mathrm{T}}\lambda_{\max}^2\left(\boldsymbol{C}\boldsymbol{A}_3\right)\boldsymbol{\xi} + k_3^{-1} \\ &\times \mathrm{tr}\left\{\tilde{\boldsymbol{W}}^{*\mathrm{T}}\hat{\boldsymbol{h}}\hat{\boldsymbol{h}}^{\mathrm{T}}\hat{\boldsymbol{W}}^{*\mathrm{T}}\right\} + 2k_4\mathrm{tr}\left\{\tilde{\boldsymbol{W}}^{*\mathrm{T}}\hat{\boldsymbol{W}}^*\right\} \\ &+ \nu_1^{-1}\bar{W}^2\bar{h}^2 + \nu_1^{-1}\mu_{\max}^2 - 2\mathrm{tr}\left\{\tilde{\boldsymbol{W}}^{*\mathrm{T}}\hat{\boldsymbol{h}}\boldsymbol{y}_1^{\mathrm{T}}\right\} \end{aligned} \tag{24}$$

where $\tilde{\Theta}_{\max} = \max\left\{\tilde{\Theta}_1, \tilde{\Theta}_2, \tilde{\Theta}_3\right\}$ and $\boldsymbol{y}_1 = \boldsymbol{C}\boldsymbol{\xi}$. Based on $\left(0.5k_3\|\tilde{\boldsymbol{W}}^*\|^2\right)^{\frac{2l-1}{l}} - 0.5k_3\|\tilde{\boldsymbol{W}}^*\|^2 \le 1$, $\tilde{\boldsymbol{W}}^{*\mathrm{T}}\hat{\boldsymbol{W}}^* = \tilde{\boldsymbol{W}}^{*\mathrm{T}}\boldsymbol{W}^* - \|\tilde{\boldsymbol{W}}^*\|^2 \le -0.5\|\tilde{\boldsymbol{W}}^*\|^2 + 0.5\bar{W}^2$, Lemma 5, (21) and $\boldsymbol{E} = \boldsymbol{B}^{\mathrm{T}} - \boldsymbol{C}\boldsymbol{A}_3$, (24) can be transformed to be

$$\begin{aligned}\dot{V}_1 \le& -a\tilde{\Theta}_{\max}^{\frac{2l-2}{l}}\boldsymbol{\xi}^{\mathrm{T}}\boldsymbol{K}_1\boldsymbol{\xi} + k_3\boldsymbol{\xi}^{\mathrm{T}}\left(\boldsymbol{C}\boldsymbol{A}_2 + \boldsymbol{A}^{\mathrm{T}}\boldsymbol{C}\right)\boldsymbol{\xi} \\ &+ \nu_1^{-1}\bar{W}^2\bar{h}^2 - 2\boldsymbol{\xi}\boldsymbol{E}\tilde{\boldsymbol{W}}^{*\mathrm{T}}\hat{\boldsymbol{h}} + \nu_1^{-1}\mu_{\max}^2 \\ &+ 2\nu\boldsymbol{\xi}^{\mathrm{T}}\lambda_{\max}^2\left(\boldsymbol{C}\boldsymbol{A}_3\right)\boldsymbol{\xi} - 0.5\left(k_4 - k_3^{-1}\bar{h}^2\right)\|\tilde{\boldsymbol{W}}^*\|^2 \\ &+ 0.5k_3^{-1}\bar{W}^2\bar{h}^2 - \left(0.5k_4\|\tilde{\boldsymbol{W}}^*\|^2\right)^{\frac{2l-1}{l}} \\ &- k_3^{-1}\boldsymbol{h}^{\mathrm{T}}(\boldsymbol{\Theta}, \hat{\boldsymbol{w}})\tilde{\boldsymbol{W}}^*\tilde{\boldsymbol{W}}^{*\mathrm{T}}\hat{\boldsymbol{h}} + k_4\bar{W}^2 + 1 \\ \le& -a\tilde{\Theta}_{\max}^{\frac{2l-2}{l}}\lambda_{\max}\left(\boldsymbol{K}_1\right)\|\boldsymbol{\xi}\|^2 - k_3\lambda_{\min}\left(\boldsymbol{K}_2\right)\|\boldsymbol{\xi}\|^2 \\ &+ 2\nu\lambda_{\max}^2\left(\boldsymbol{C}\boldsymbol{A}_3\right)\|\boldsymbol{\xi}\|^2 - 0.5\left(k_4 - k_3^{-1}\bar{h}^2\right)\|\tilde{\boldsymbol{W}}^*\|^2 \\ &- \left(0.5k_4\|\tilde{\boldsymbol{W}}^*\|^2\right)^{\frac{2l-1}{l}} + \nu_1^{-1}\bar{W}^2\bar{h}^2 + \nu_1^{-1}\mu_{\max}^2 \\ &+ 0.5k_3^{-1}\bar{W}^2\bar{h}^2 + k_4\bar{W}^2 + 1. \end{aligned} \tag{25}$$

Since $\frac{2l-2}{l} < 0$ and $\tilde{\Theta}_{\max} \le \|\tilde{\boldsymbol{\Theta}}\| \le k_3^{-1}\|\boldsymbol{y}_1\| \le k_3^{-1}\|\boldsymbol{\xi}\|$, one can get that $\left(k_3^{-1}\|\boldsymbol{\xi}\|\right)^{\frac{2l-2}{l}} \le \tilde{\Theta}_{\max}^{\frac{2l-2}{l}}$. In view of Lemma 2, (25) is rewritten as

$$\begin{aligned}\dot{V}_1 \le& -a\lambda_{\max}\left(\boldsymbol{K}_1\right)k_3^{\frac{2-2l}{l}}\|\boldsymbol{\xi}\|^{\frac{4l-2}{l}} - \left(0.5k_4\right)^{\frac{2l-1}{l}}\|\tilde{\boldsymbol{W}}^*\|^{\frac{4l-2}{l}} \\ &- \left(k_3\lambda_{\min}\left(\boldsymbol{K}_2\right) - 2\nu\lambda_{\max}^2\left(\boldsymbol{C}\boldsymbol{A}_3\right)\right)\|\boldsymbol{\xi}\|^2 \\ &- 0.5\left(k_4 - k_3^{-1}\bar{h}^2\right)\|\tilde{\boldsymbol{W}}^*\|^2 + \Delta_1 \\ \le& -\Psi_1 V_1 - \Psi_2 V_1^{\frac{2l-1}{l}} + \Delta_1 \end{aligned} \tag{26}$$

as long as $k_3 > \left(2\nu\lambda_{\max}^2(\boldsymbol{C}\boldsymbol{A}_3)\right)/\left(k_3\lambda_{\min}(\boldsymbol{K}_2)\right)$ and $k_4 > \left(\bar{h}^2/k_3\right)$, the inequality (26) will be satisfied. Meanwhile, $\Psi_1 = \min\left\{a\lambda_{\max}\left(\boldsymbol{K}_1\right)\ k_3^{\frac{2-2l}{l}}, \left(0.5k_4\right)^{\frac{2l-1}{l}}\right\}$, $\Psi_2 = \min\left\{k_3\lambda_{\min}\left(\boldsymbol{K}_2\right) - 2\nu\lambda_{\max}^2\left(\boldsymbol{C}\boldsymbol{A}_3\right), 0.5\left(k_4 - k_3^{-1}\bar{h}^2\right)\right\}$ and $\Delta_1 = \nu_1^{-1}\mu_{\max}^2 + 0.5k_3^{-1}\bar{W}^2\bar{h}^2 + k_4\bar{W}^2 + 1$.

Afterwards, we can transform (26) into the following:

$$\dot{V}_1 \le -\Psi_1\Xi_1 V_1 - (1 - \Xi_1)\Psi_1 V_1 - \Psi_2 V_1^{\frac{2l-1}{l}} + \Delta_1 \tag{27}$$

or

$$\dot{V}_1 \le -\Psi_1 V_1 - \Xi_1\Psi_2 V_1^{\frac{2l-1}{l}} - (1 - \Xi_1)\Psi_2 V_1^{\frac{2l-1}{l}} + \Delta_1 \tag{28}$$

where $0 < \Xi_1 < 1$. Based on (27) and (28), it follows that when the function V_1 satisfies $V_1 \ge \Delta_1/\left(\Psi_1(1 - \Xi_1)\right)$, then $\dot{V}_1 \le -\Psi_1\Xi_1 V_1 - \Psi_2 V_1^{\frac{2l-1}{l}}$; and when the function V_1 satisfies $\Delta_1/\left((1-\Xi_1)\Psi_2\right)^{\frac{l}{2l-1}}$, then $\dot{V}_1 \le -\Psi_1 V_1 - \Xi_1\Psi_2 V_1^{\frac{2l-1}{l}}$. Thus, based on Lemma 3, it can be obtained that the function V_1 shall converge into the following region, as

$$V_1 \le \min\left\{\frac{\Delta_1}{\Psi_1(1 - \Xi_1)}, \frac{\Delta_1}{\left((1 - \Xi_1)\Psi_2\right)^{l/(2l-1)}}\right\}. \tag{29}$$

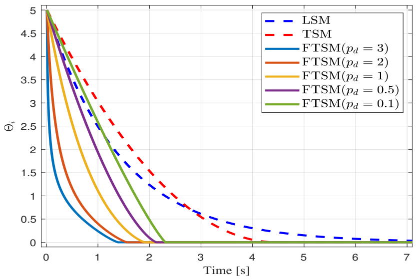

Fig. 4. Comparison of convergence speeds of LSM, TSM, and FTSM surfaces

By letting $\Omega_1 = \Delta_1/\big(\Psi_1(1-\Xi_1)\big)$ and $\Omega_2 = \Delta_1/\big((1-\Xi_1)\Psi_2\big)^{\frac{l}{2l-1}}$, it follows that $\tilde{\boldsymbol{\Theta}}$, $\tilde{\boldsymbol{w}}$ and $\tilde{\boldsymbol{W}}^*$ will drive into the following regions, as

$$\begin{cases} \|\tilde{\boldsymbol{\Theta}}\| \leq k_3^{-1}\lambda_{\min}^{-\frac{1}{2}}(\boldsymbol{C})\min\{\Omega_1,\Omega_2\} \\ \|\tilde{\boldsymbol{w}}\| \leq \lambda_{\min}^{-\frac{1}{2}}(\boldsymbol{C})\min\{\Omega_1,\Omega_2\} \\ \|\tilde{\boldsymbol{W}}^*\| \leq \lambda_{\min}^{-\frac{1}{2}}(\boldsymbol{\Upsilon}^{-1})\min\{\Omega_1,\Omega_2\} \end{cases} \tag{30}$$

and the setting time t is bounded by

$$t \leq t_0 + \max\left\{\frac{l}{\Xi_1\Psi_1(1-l)}\ln\frac{\Xi_1\Psi_1V_1^{(1-l)/l}(t_0)+\Psi_2}{\Psi_2}, \frac{l}{\Psi_1(1-l)}\ln\frac{\Psi_1V_1^{(1-l)/l}(t_0)+\Xi_1\Psi_2}{\Xi_1\Psi_2}\right\}. \tag{31}$$

where t_0 is the initial time. Consequently, this completes proof.

B. Controller Development

Since the signals $\boldsymbol{\Theta}$ and $\dot{\boldsymbol{\Theta}}$ can be substituted by their estimations $\hat{\boldsymbol{\Theta}}$ and $\dot{\hat{\boldsymbol{\Theta}}}$, the estimated errors can be written by

$$\boldsymbol{\Theta}_e = \hat{\boldsymbol{\Theta}} - \boldsymbol{\Theta}_d,\ \dot{\boldsymbol{\Theta}}_e = \hat{\boldsymbol{w}} - \dot{\boldsymbol{\Theta}}_d \tag{32}$$

where $\boldsymbol{\Theta}_d$ and $\dot{\boldsymbol{\Theta}}_d$ are the desired attitude signal and its first-order derivative. Then, a NFTSM surface is introduced as

$$\boldsymbol{s}_n = \boldsymbol{\Theta}_e + \beta_a\mathrm{sign}(\boldsymbol{\Theta}_e)^{m_c} + \beta_b\mathrm{sign}\big(\dot{\boldsymbol{\Theta}}_e\big)^{\frac{m_a}{m_b}} \tag{33}$$

where $\boldsymbol{s}_n = \big[s_{n,1}; s_{n,2}; s_{n,3}\big]$ expresses the NFTSM surface, $\beta_a > 0$, $\beta_b > 0$, and m_a and m_b denote positive odd integers with $1 < \frac{m_a}{m_b} < 2$ and $m_c > \frac{m_a}{m_b}$.

Remark 4: The mathematical expressions of LSM, TSM and FTSM surfaces are described by

$$\text{LSM surface:}\quad \boldsymbol{s}_l = \beta_c\boldsymbol{\Theta}_e + \dot{\boldsymbol{\Theta}}_e \tag{34a}$$

$$\text{TSM surface:}\quad \boldsymbol{s}_t = \beta_d\boldsymbol{\Theta}_e + \dot{\boldsymbol{\Theta}}_e^{\frac{p_0}{q_0}} \tag{34b}$$

$$\text{FTSM surface:}\ \boldsymbol{s}_f = \dot{\boldsymbol{\Theta}}_e + p_a\mathrm{sign}(\boldsymbol{\Theta}_e)^{p_c} + p_b\mathrm{sign}(\boldsymbol{\Theta}_e)^{p_d} \tag{34c}$$

where $\beta_c > 0$, $\beta_d > 0$, $p_a > 0$, $p_b > 0$, $p_c \geq 1$, $0 < p_d < 1$, and $p_0 > 0$ and $q_0 > 0$ denote odd numbers with $0 < p_0/q_0 < 1$. When the state is close to the equilibrium, $\boldsymbol{\Theta}_e$ ensures fast transient convergence. When the state is far from the equilibrium, the term $p_a\mathrm{sign}(\boldsymbol{\Theta}_e)^{p_c}$ would accelerate the error $\boldsymbol{\Theta}_e$ to zero. From Fig. 4, it can be observed that FTSM provides a faster convergence speed than that of LSM and TSM surfaces, and the convergence speed of the FTSM surface can be accelerated by selecting a larger value p_d. Furthermore, in contrast to the FTSM surface, the NFTSM surface can solve the singularity problem due to the fractional order $\frac{m_a}{m_b} - 1 > 0$.

The derivative of (33) along (5) is first formulated as

$$\dot{\boldsymbol{s}}_n = \dot{\boldsymbol{\Theta}}_e + \beta_a m_c|\boldsymbol{\Theta}_e|^{m_c-1}\dot{\boldsymbol{\Theta}}_e + \beta_b\frac{m_a}{m_b}\big|\dot{\boldsymbol{\Theta}}_e\big|^{\frac{m_a}{m_b}-1} + \boldsymbol{N}_1^{-1} \times \Big(-\boldsymbol{N}_2\dot{\hat{\boldsymbol{\Theta}}} - \boldsymbol{N}_1\ddot{\boldsymbol{\Theta}}_d + \boldsymbol{R}_t^{\mathrm{T}}\boldsymbol{E}\mathrm{sat}(\boldsymbol{u}) + \boldsymbol{D}\Big). \tag{35}$$

The equivalent controller $\boldsymbol{u}_{o,eq}$ can be obtained by solving (35) without consideration of $\boldsymbol{D}$, as

$$\boldsymbol{u}_{o,eq} = -\boldsymbol{P}_2^{-1}\Bigg(\frac{\beta_a m_c m_b}{\beta_b m_a}\mathrm{diag}\Big\{|\boldsymbol{\Theta}_e|^{m_c-1}\Big\}\mathrm{sign}\big(\dot{\boldsymbol{\Theta}}_e\big)^{2-\frac{m_a}{m_b}} + \frac{m_a}{m_b\beta_b}\mathrm{sign}\big(\dot{\boldsymbol{\Theta}}_e\big)^{2-\frac{m_a}{m_b}} + \boldsymbol{P}_1\dot{\hat{\boldsymbol{\Theta}}} - \ddot{\boldsymbol{\Theta}}_d\Bigg). \tag{36}$$

where $\boldsymbol{P}_1 = \boldsymbol{N}_1^{-1}\boldsymbol{N}_2$ and $\boldsymbol{P}_2 = \boldsymbol{N}_1^{-1}\boldsymbol{R}_t^{\mathrm{T}}$. Since $\boldsymbol{N}_1^{-1}$ and $\boldsymbol{N}_2^{-1}$ described in (5) are nonsingular and based on the definition of $\boldsymbol{R}_t$, it is not hard to know that $\boldsymbol{P}_1^{-1}$ and $\boldsymbol{P}_2^{-1}$ are nonsingular.

Since the lumped disturbance is inevitable in practice, this study puts forward the following switching controller, as

$$\begin{cases} \boldsymbol{u}_{o,sw} = -\boldsymbol{P}_2^{-1}\big(\boldsymbol{u}_{o,sw,1} + \boldsymbol{u}_{o,sw,2}\big) \\ \boldsymbol{u}_{o,sw,1} = k_a\boldsymbol{s}_n + k_b\mathrm{sign}(\boldsymbol{s}_n)^{\frac{k_c}{k_d}} \\ \boldsymbol{u}_{o,sw,2} = \boldsymbol{r}_a(\boldsymbol{v}_1 - \boldsymbol{v}_3) \end{cases} \tag{37}$$

where $\boldsymbol{u}_{o,sw,1}$ is a fast switching control part, $k_a > 0$ and $k_b > 0$, $k_c > 0$ and $k_d > 0$ denote odd integers with $k_c < k_d$; $\boldsymbol{u}_{o,sw,2}$ is a fuzzy logic inference mechanism part.

To overcome the problem of the input saturation, this article presents an auxiliary system with the following form:

$$\dot{\boldsymbol{\chi}} = -n_a\boldsymbol{\chi} - n_b\boldsymbol{\chi}^{\frac{m_a}{m_b}} - \frac{\big(\Xi(\boldsymbol{\chi})+\frac{1}{2}\big)\big(\boldsymbol{s}_n^{\mathrm{T}}\boldsymbol{s}_n + \Delta\boldsymbol{u}^{\mathrm{T}}\Delta\boldsymbol{u}\big)}{2\|\boldsymbol{\chi}\|^2}\boldsymbol{\chi} + \Delta\boldsymbol{u} \tag{38}$$

with a smooth and nonsingular function $\Xi(\boldsymbol{\chi})$ being

$$\Xi(\boldsymbol{\chi}) = \begin{cases} 0, & \|\boldsymbol{\chi}\| \leq \delta_a \\ 1, & \|\boldsymbol{\chi}\| \geq \delta_b \\ 1-\cos\left(\frac{\pi}{2}\sin\left(\frac{\pi}{2}\frac{\|\boldsymbol{\chi}\|^2-\delta_a}{\delta_b^2-\delta_a^2}\right)\right), & \text{otherwise} \end{cases} \tag{39}$$

where $n_a > 1$ and $n_b > 0$; $\delta_a > 0$ and $\delta_b > 0$ are arbitrarily small design constants; $\Delta\boldsymbol{u} = \boldsymbol{u}_o - \mathrm{sat}(\boldsymbol{u})$. Therefore, the saturation compensation controller $\boldsymbol{u}_{o,sa}$ is constructed by

$$\boldsymbol{u}_{o,sa} = \boldsymbol{P}_2^{-1}\boldsymbol{\chi}. \tag{40}$$

By recalling the previous development, the composite attitude control law is given by

$$\boldsymbol{u}_o = \boldsymbol{u}_{o,eq} + \boldsymbol{u}_{o,sw} + \boldsymbol{u}_{o,sa}. \tag{41}$$

Since the upper bound of the lumped uncertainty is hard to obtain accurately, a larger $\boldsymbol{r}_a$ needs to be chosen. Unfortunately, this causes more energy consumption and chattering. To overcome this challenge, this article develops the following adaptive mechanism to update the parameter $\boldsymbol{r}_a$:

$$\dot{\hat{\boldsymbol{r}}}_a = \frac{\beta_b m_a}{m_b}\mathrm{diag}\left\{\big|\dot{\boldsymbol{\Theta}}_e\big|^{\frac{m_a}{m_b}-1}\right\}\frac{(\boldsymbol{v}_1-\boldsymbol{v}_3)\boldsymbol{s}_n}{\sigma} - \mu_1\hat{\boldsymbol{r}}_a - \mu_2\hat{\boldsymbol{r}}_a^{\mu_3} \tag{42}$$

where $\hat{\boldsymbol{r}}_a = \big[\hat{r}_{a,1};\hat{r}_{a,2};\hat{r}_{a,3}\big]$, $\hat{r}_{a,i}(0) \geq 0$, $\mu_1 > 0$, $\mu_2 > 0$, $0 < \mu_3 < 1$, and $\sigma > 0$ can adjust the estimation rate of $\hat{\boldsymbol{r}}_a$. From (41) and (42), an observer-based adaptive fuzzy finite-time attitude controller can be deduced to the following

$$\begin{aligned}\boldsymbol{u}_o = &-\boldsymbol{P}_2^{-1}\Big(\frac{\beta_a m_c m_b}{\beta_b m_a}\mathrm{diag}\Big\{\big|\boldsymbol{\Theta}_e\big|^{m_c-1}\Big\}\mathrm{sign}\big(\dot{\boldsymbol{\Theta}}_e\big)^{2-\frac{m_a}{m_b}}\\&+\frac{m_a}{m_b\beta_b}\mathrm{sign}\big(\dot{\boldsymbol{\Theta}}_e\big)^{2-\frac{m_a}{m_b}}+\boldsymbol{P}_1\dot{\boldsymbol{\Theta}}-\ddot{\boldsymbol{\Theta}}_d+k_a\boldsymbol{s}_n\\&+k_b\mathrm{sign}(\boldsymbol{s}_n)^{\frac{k_c}{k_d}}+(\boldsymbol{v}_1-\boldsymbol{v}_3)\hat{\boldsymbol{r}}_a-\boldsymbol{\chi}\Big).\end{aligned}\tag{43}$$

Theorem 2: For the attitude system (5), the proposed attitude control law in (38), (39), (42) and (43) can guarantee that all the system signals can bounded and tracking errors converge to sufficiently small bounded regions in finite time.

Proof: Select a composite Lyapunov function as

$$\begin{aligned}V_2 = &\boldsymbol{\xi}^{\mathrm{T}}\boldsymbol{C}\boldsymbol{\xi}+\mathrm{tr}\Big\{\tilde{\boldsymbol{W}}^{*\mathrm{T}}\boldsymbol{\Upsilon}^{-1}\tilde{\boldsymbol{W}}^{*\mathrm{T}}\Big\}\\&+\frac{1}{2}\boldsymbol{s}_n^{\mathrm{T}}\boldsymbol{s}_n+\frac{1}{2}\boldsymbol{\chi}^{\mathrm{T}}\boldsymbol{\chi}+\frac{\sigma}{2}\sum_{i=1}^{3}\tilde{r}_{a,i}^2\end{aligned}\tag{44}$$

where $\tilde{r}_{a,i} = \hat{r}_{a,i} - \bar{r}_{a,i}$ denotes the estimation error, and $\bar{r}_{a,i}$ is the upper bound of $\hat{r}_{a,i}$. Without loss of generality, $\bar{r}_{a,i}$ is suppose to be $\bar{r}_{a,i} = \left|\frac{\bar{D}}{c_1-c_3}\right| + r_{0,i}$, and in which $r_{0,i}$ is a very small positive constant and belongs to an element of $\boldsymbol{r}_o \in \mathbb{R}^3$.

The stability analysis are give by the following three cases.

Case 1: For $\|\boldsymbol{\xi}\| \geq \delta_b$, i.e., $\Xi(\boldsymbol{\xi}) = 1$. Substituting (43) into the derivative of (44), and using the Lemma 1 that $\boldsymbol{s}_n^{\mathrm{T}}\boldsymbol{\chi} \leq \frac{3}{2}\boldsymbol{s}_n^{\mathrm{T}}\boldsymbol{s}_n + \frac{1}{6}\boldsymbol{\chi}^{\mathrm{T}}\boldsymbol{\chi}$ and $\boldsymbol{\chi}^{\mathrm{T}}\Delta\boldsymbol{u} \leq \frac{1}{6}\boldsymbol{\chi}^{\mathrm{T}}\boldsymbol{\chi} + \frac{3}{2}\Delta\boldsymbol{u}^{\mathrm{T}}\Delta\boldsymbol{u}$, yield

$$\begin{aligned}\dot{V}_2 \leq &\boldsymbol{s}_n^{\mathrm{T}}\Big\{\dot{\boldsymbol{\Theta}}_e+\beta_a m_c\mathrm{diag}\big(|\boldsymbol{\Theta}_e|^{m_c-1}\big)\dot{\boldsymbol{\Theta}}_e-\mathrm{diag}\Big(\big|\dot{\boldsymbol{\Theta}}_e\big|^{\frac{m_a}{m_b}-1}\Big)\\&\times\Big[-\beta_a m_c\mathrm{diag}(|\boldsymbol{\Theta}_e|^{m_c-1})\mathrm{sign}(\dot{\boldsymbol{\Theta}}_e)^{2-\frac{m_a}{m_b}}-\frac{\beta_b m_a}{m_b}\Big(k_a\boldsymbol{s}_n\\&+k_b\mathrm{sign}(\boldsymbol{s}_n)^{\frac{k_c}{k_d}}-\boldsymbol{D}+(\boldsymbol{v}_1-\boldsymbol{v}_3)\hat{\boldsymbol{r}}_a\Big)+\mathrm{sign}(\dot{\boldsymbol{\Theta}}_e)^{2-\frac{m_a}{m_b}}\Big]\Big\}\\&-n_a\boldsymbol{\chi}^{\mathrm{T}}\boldsymbol{\chi}-n_b\boldsymbol{\chi}^{\mathrm{T}}\boldsymbol{\chi}^{\frac{k_c}{k_d}}+\boldsymbol{s}_n^{\mathrm{T}}\boldsymbol{\chi}-\frac{3}{2}\Delta\boldsymbol{u}^{\mathrm{T}}\Delta\boldsymbol{u}-\frac{3}{2}\boldsymbol{s}_n^{\mathrm{T}}\boldsymbol{s}_n\\&+\boldsymbol{\chi}^{\mathrm{T}}\Delta\boldsymbol{u}-\Psi_1V_1-\Psi_2V_1^{\frac{2l-1}{l}}+\tilde{\boldsymbol{r}}_a^{\mathrm{T}}\Big(\mathrm{diag}\Big\{\big|\dot{\boldsymbol{\Theta}}_e\big|^{\frac{m_a}{m_b}-1}\Big\}\\&\times\big((\boldsymbol{v}_1-\boldsymbol{v}_3)\big)\boldsymbol{s}_n\Big)\frac{\beta_b m_a}{m_b}-\sigma\mu_1\sum_{i=1}^{3}\tilde{r}_{a,i}\hat{r}_{a,i}\\&-\sigma\mu_1\sum_{i=1}^{3}\tilde{r}_{a,i}\hat{r}_{a,i}^{\mu_3}+\Delta_1\\\leq &-\frac{\beta_b m_a}{m_b}\boldsymbol{s}_n^{\mathrm{T}}\mathrm{diag}\Big(\big|\dot{\boldsymbol{\Theta}}_e\big|^{\frac{m_a}{m_b}-1}\Big)\Big(k_a\boldsymbol{s}_n+k_b\mathrm{sign}(\boldsymbol{s}_n)^{\frac{k_c}{k_d}}\\&-\boldsymbol{D}+(\boldsymbol{v}_1-\boldsymbol{v}_3)\hat{\boldsymbol{r}}_a\Big)-\Big(n_a-\frac{1}{3}\Big)\boldsymbol{\chi}^{\mathrm{T}}\boldsymbol{\chi}-n_b\boldsymbol{\chi}^{\mathrm{T}}\boldsymbol{\chi}^{\frac{k_c}{k_d}}\\&+\tilde{\boldsymbol{r}}_a^{\mathrm{T}}\Big(\frac{\beta_b m_a}{m_b}\mathrm{diag}\Big(\big|\dot{\boldsymbol{\Theta}}_e\big|^{\frac{m_a}{m_b}-1}\Big)\big((\boldsymbol{v}_1-\boldsymbol{v}_3)\boldsymbol{s}_n\big)\Big)-\Psi_1V_1\\&-\Psi_2V_1^{\frac{2l-1}{l}}-\sigma\mu_1\sum_{i=1}^{3}\tilde{r}_{a,i}\hat{r}_{a,i}-\sigma\mu_1\sum_{i=1}^{3}\tilde{r}_{a,i}\hat{r}_{a,i}^{\mu_3}+\Delta_1.\end{aligned}\tag{45}$$

By taking $\boldsymbol{s}_n$ as the input of FLS, it follows that each element of $\boldsymbol{s}_n^{\mathrm{T}}(\boldsymbol{v}_1-\boldsymbol{v}_3)$ is positive. Thus, one has

$$\begin{aligned}-\boldsymbol{s}_n^{\mathrm{T}}&(\boldsymbol{v}_1-\boldsymbol{v}_3)\boldsymbol{r}_a+\boldsymbol{s}_n^{\mathrm{T}}\boldsymbol{D}=\\&-\boldsymbol{s}_n^{\mathrm{T}}(\boldsymbol{v}_1-\boldsymbol{v}_3)\Big(\boldsymbol{r}_a-\frac{1}{\boldsymbol{v}_1-\boldsymbol{v}_3}\boldsymbol{D}\Big).\end{aligned}\tag{46}$$

By adding and subtracting $(\boldsymbol{v}_1-\boldsymbol{v}_3)\bar{\boldsymbol{r}}_a$ to the right-hand side of (45), and using (46), (45) can hence be formulated as

$$\begin{aligned}\dot{V}_2 \leq &-\frac{\beta_b m_a}{m_b}\boldsymbol{s}_n^{\mathrm{T}}\mathrm{diag}\Big(\big|\dot{\boldsymbol{\Theta}}_e\big|^{\frac{m_a}{m_b}-1}\Big)\Big(k_a\boldsymbol{s}_n+k_b\mathrm{sign}(\boldsymbol{s}_n)^{\frac{k_c}{k_d}}\\&-\boldsymbol{D}+(\boldsymbol{v}_1-\boldsymbol{v}_3)\hat{\boldsymbol{r}}_a+(\boldsymbol{v}_1-\boldsymbol{v}_3)\bar{\boldsymbol{r}}_a-(\boldsymbol{v}_1-\boldsymbol{v}_3)\bar{\boldsymbol{r}}_a\Big)\\&-\Big(n_a-\frac{1}{3}\Big)\boldsymbol{\chi}^{\mathrm{T}}\boldsymbol{\chi}-n_b\boldsymbol{\chi}^{\mathrm{T}}\boldsymbol{\chi}^{\frac{k_c}{k_d}}-\Psi_1V_1-\Psi_2V_1^{\frac{2l-1}{l}}\\&+\tilde{\boldsymbol{r}}_a^{\mathrm{T}}\Big(\frac{\beta_b m_a}{m_b}\mathrm{diag}\Big(\big|\dot{\boldsymbol{\Theta}}_e\big|^{\frac{m_a}{m_b}-1}\Big)\big((\boldsymbol{v}_1-\boldsymbol{v}_3)\boldsymbol{s}_n\big)\Big)\\&-\sigma\mu_1\sum_{i=1}^{3}\tilde{r}_{a,i}\hat{r}_{a,i}-\sigma\mu_2\sum_{i=1}^{3}\tilde{r}_{a,i}\hat{r}_{a,i}^{\mu_3}+\Delta_1\\=&-\frac{\beta_b m_a}{m_b}\boldsymbol{s}_n^{\mathrm{T}}\mathrm{diag}\Big(\big|\dot{\boldsymbol{\Theta}}_e\big|^{\frac{m_a}{m_b}-1}\Big)\Big(k_b\mathrm{sign}(\boldsymbol{s}_n)^{\frac{k_c}{k_d}}+\tilde{\boldsymbol{r}}_a(\boldsymbol{v}_1\\&-\boldsymbol{v}_3)+k_a\boldsymbol{s}_n\Big)-\Big(n_a-\frac{1}{3}\Big)\boldsymbol{\chi}^{\mathrm{T}}\boldsymbol{\chi}-n_b\boldsymbol{\chi}^{\mathrm{T}}\boldsymbol{\chi}^{\frac{k_c}{k_d}}-\Psi_1V_1\\&-\Psi_2V_1^{\frac{2l-1}{l}}+\tilde{\boldsymbol{r}}_a^{\mathrm{T}}\Big(\frac{\beta_b m_a}{m_b}\mathrm{diag}\Big(\big|\dot{\boldsymbol{\Theta}}_e\big|^{\frac{m_a}{m_b}-1}\Big)\big((\boldsymbol{v}_1-\boldsymbol{v}_3)\\&\times\boldsymbol{s}_n\big)\Big)-\sigma\mu_2\sum_{i=1}^{3}\tilde{r}_{a,i}\hat{r}_{a,i}^{\mu_3}-\boldsymbol{r}_0^{\mathrm{T}}\Big(\frac{\beta_b m_a}{m_b}\mathrm{diag}\Big(\big|\dot{\boldsymbol{\Theta}}_e\big|^{\frac{m_a}{m_b}-1}\Big)\\&\times\big((\boldsymbol{v}_1-\boldsymbol{v}_3)\boldsymbol{s}_n\big)\Big)-\sigma\mu_1\sum_{i=1}^{3}\tilde{r}_{a,i}\hat{r}_{a,i}+\Delta_1.\end{aligned}\tag{47}$$

Now recalling Lemmas 1 and 5, one can derive

$$-\sigma\mu_1\tilde{r}_{a,i}\hat{r}_{a,i} \leq -\frac{\sigma\mu_1}{2}\tilde{r}_{a,i}^2+\frac{\sigma\mu_1}{2}\bar{r}_{a,i}^2,\tag{48a}$$

$$-\sigma\mu_2\tilde{r}_{a,i}\hat{r}_{a,i}^{\mu_3} \leq -\frac{\sigma\mu_2(1-\mu_4)}{(1+\mu_3)}\tilde{r}_{a,i}^{1+\mu_3}+\frac{\sigma\mu_2 \upsilon_i}{1+\mu_3}\tag{48b}$$

where $0 < \mu_4 < 1$ and $\upsilon_i = \bar{r}_{a,i} + \Big(\frac{\bar{r}_{a,i}}{1-(1-\mu_4)^{1/(1+\mu_3)}}\Big)^{1+\mu_3} + \Big(\frac{\bar{r}_{a,i}(1-\mu_4)^{1/(1+\mu_3)}}{1-(1-\mu_4)^{1/(1+\mu_3)}}\Big)^{1+\mu_3}$.

Combining (47) and (48), leads to

$$\begin{aligned}\dot{V}_2 \leq &-\lambda_{\min}(\boldsymbol{L}_1)\boldsymbol{s}_n^{\mathrm{T}}\boldsymbol{s}_n-\lambda_{\min}(\boldsymbol{L}_2)\|\boldsymbol{s}_n\|^{\frac{k_c+k_d}{k_d}}-n_b\|\boldsymbol{\chi}\|^{\frac{k_c+k_d}{k_d}}\\&-\Big(n_a-\frac{1}{3}\Big)\boldsymbol{\chi}^{\mathrm{T}}\boldsymbol{\chi}-\Psi_1V_1-\Psi_2V_1^{\frac{2l-1}{l}}-\frac{\sigma\mu_2(1-\mu_4)}{(1+\mu_3)}\\&\times\sum_{i=1}^{3}\tilde{r}_{a,i}^{1+\mu_3}-\frac{\sigma\mu_1}{2}\sum_{i=1}^{3}\tilde{r}_{a,i}^2+\frac{\sigma\mu_1}{2}\sum_{i=1}^{3}\bar{r}_{a,i}^2+\Delta_1\\\leq &-L_3V_2-L_4V_2^{\frac{2l-1}{l}}+\Delta_2\end{aligned}\tag{49}$$

where $n_a > \frac{1}{3}$, $\frac{2l-1}{l} = \frac{k_c+k_d}{2k_d}$, $\boldsymbol{L}_1 = \frac{k_a\beta_b m_a}{m_b}\boldsymbol{s}_n^{\mathrm{T}}\mathrm{diag}\Big(\big|\dot{\boldsymbol{\Theta}}_e\big|^{\frac{m_a}{m_b}-1}\Big)$, $\boldsymbol{L}_2 = \frac{k_b}{k_a}\boldsymbol{L}_1$, $L_3 = \min\big\{2\lambda_{\min}(\boldsymbol{L}_1), 2\big(n_a - \frac{1}{3}\big), \Psi_1, \mu_1\big\}$, $L_4 = \min\Big\{2^{\frac{k_c+k_d}{2k_d}}\lambda_{\min}(\boldsymbol{L}_2), 2^{\frac{k_c+k_d}{2k_d}}n_b, \Psi_2, \frac{2\mu_2(1-\mu_4)}{(1+\mu_3)}\Big\}$, $\mu_3 = 3 - \frac{2}{l}$, and $\Delta_2 = \Delta_1 + \frac{\sigma\mu_1}{2}\sum_{i=1}^{3}\bar{r}_{a,i}^2 + \sigma\mu_2\sum_{i=1}^{3}\upsilon_i$.

Case 2: For $\|\boldsymbol{\xi}\| \geq \delta_a$, i.e., $\Xi(\boldsymbol{\xi}) = \mathbf{0}$, the inequality (47) can be rewritten as

$$\begin{aligned}\dot{V}_2 \leq &-\lambda_{\min}(\boldsymbol{L}_1)\boldsymbol{s}_n^{\mathrm{T}}\boldsymbol{s}_n - \lambda_{\min}(\boldsymbol{L}_2)\|\boldsymbol{s}_n\|^{\frac{k_c+k_d}{k_d}} - n_b\|\boldsymbol{\chi}\|^{\frac{k_c+k_d}{k_d}} \\ &-(n_a-1)\boldsymbol{\chi}^{\mathrm{T}}\boldsymbol{\chi} - \Psi_1 V_1 - \Psi_2 V_1^{\frac{2l-1}{l}} - \frac{\sigma\mu_1}{2}\sum_{i=1}^{3}\tilde{r}_{a,i}^2 \\ &-\frac{\sigma\mu_2(1-\mu_4)}{(1+\mu_3)}\sum_{i=1}^{3}\tilde{r}_{a,i}^{1+\mu_3} + \frac{\sigma\mu_1}{2}\sum_{i=1}^{3}\bar{r}_{a,i}^2 + \Delta_1 \\ \leq &-L_5 V_2 - L_4 V_2^{\frac{2l-1}{l}} + \Delta_2 \end{aligned} \tag{50}$$

where $L_5 = \min\{2\lambda_{\min}(\boldsymbol{L}_1), 2(n_a-1), \Psi_1, \mu_1\}$, $\mu_3 = 3 - \frac{2}{l}$, and $\Delta_2 = \Delta_1 + \frac{\sigma\mu_1}{2}\sum_{i=1}^{3}\bar{r}_{a,i}^2 + \sigma\mu_2\sum_{i=1}^{3}\upsilon_i$.

Case 3: For the remaining case, it has $\Xi(\boldsymbol{\chi}) \in (0,1)$. Based on the previous analysis, one can get the similar result, as

$$\begin{aligned}\dot{V}_2 \leq &-\lambda_{\min}(\boldsymbol{L}_1)\boldsymbol{s}_n^{\mathrm{T}}\boldsymbol{s}_n - \lambda_{\min}(\boldsymbol{L}_2)\|\boldsymbol{s}_n\|^{(k_c+k_d)/k_d} \\ &-\left(n_a - \left(\frac{1}{4\left(\Xi(\boldsymbol{\chi})+\frac{1}{2}\right)} + \Xi(\boldsymbol{\chi}) + \frac{1}{2}\right)\right)\boldsymbol{\chi}^{\mathrm{T}}\boldsymbol{\chi} \\ &-n_b\|\boldsymbol{\chi}\|^{\frac{k_c+k_d}{k_d}} - \frac{\sigma\mu_2(1-\mu_4)}{(1+\mu_3)}\sum_{i=1}^{3}\tilde{r}_{a,i}^{1+\mu_3} - \frac{\sigma\mu_1}{2}\sum_{i=1}^{3}\tilde{r}_{a,i}^2 \\ &+\frac{\sigma\mu_1}{2}\sum_{i=1}^{3}\bar{r}_{a,i}^2 + \Delta_1 - \Psi_1 V_1 - \Psi_2 V_1^{\frac{2l-1}{l}} \\ \leq &-L_6 V_2 - L_4 V_2^{\frac{2l-1}{l}} + \Delta_2 \end{aligned} \tag{51}$$

where $L_6 = \min\Big\{2\lambda_{\min}(\boldsymbol{L}_1), 2\Big(\frac{1}{4\left(\Xi(\boldsymbol{\chi})+\frac{1}{2}\right)} + \Xi(\boldsymbol{\chi}) + \frac{1}{2}\Big), \Psi_1, \mu_1\Big\}$, $\mu_3 = 3 - \frac{2}{l}$, and $\Delta_2 = \Delta_1 + \frac{\sigma\mu_1}{2}\sum_{i=1}^{3}\bar{r}_{a,i}^2 + \sigma\mu_2\sum_{i=1}^{3}\upsilon_i$. For the analysis of (49)–(51), one gets

$$\dot{V}_2 \leq -L^* V_2 - L_4 V_2^{\frac{2l-1}{l}} + \Delta_2 \tag{52}$$

where $L^* = \max\{L_3, L_5, L_6\} \geq 1$.

According to (52), it is equivalent to the following:

$$\dot{V}_2 \leq -\Xi_2 L^* V_2 - (1-\Xi_2)L^* V_2 - L_4 V_2^{\frac{2l-1}{l}} + \Delta_2 \tag{53}$$

or

$$\dot{V}_2 \leq -L^* V_2 - \Xi_2 L_4 V_2^{\frac{2l-1}{l}} - (1-\Xi_2)L_4 V_2^{\frac{2l-1}{l}} + \Delta_2 \tag{54}$$

where $0 < \Xi_2 < 1$.

On one hand, it follows from (53) that when $V_2 \geq \Delta_2/\big((1-\Xi_2)L^*\big)$, then $\dot{V}_2 \leq -\Xi_2 L^* V_3 - L_4 V_3^{[(2l-1)/l]}$. Based on Lemma 3, one can know that all the system signals will drive into the following

$$\begin{cases} \|\tilde{\boldsymbol{\Theta}}\| \leq k_3^{-1}\lambda_{\min}^{-\frac{1}{2}}(\boldsymbol{C})\sqrt{\Omega_3}, & \|\tilde{\boldsymbol{w}}\| \leq \lambda_{\min}^{-\frac{1}{2}}(\boldsymbol{C})\sqrt{\Omega_3}, \\ \|\tilde{\boldsymbol{W}}^*\| \leq \lambda_{\min}^{-\frac{1}{2}}(\boldsymbol{\Upsilon}^{-1})\sqrt{\Omega_3}, & \|\boldsymbol{s}_n\| \leq \sqrt{2}\sqrt{\Omega_3}, \\ |\tilde{r}_{a,i}| \leq \frac{\sqrt{2\sigma}}{\sigma}\sqrt{\Omega_3} \end{cases} \tag{55}$$

where $\Omega_3 = \big(\Delta_2/(1-\Xi_2)L^*\big)$, and the convergence time T_1 is bounded by

$$T_1 \leq T_0 + \frac{l}{\Xi_2 L^*(1-l)}\ln\left(\frac{\Xi_2 L^* V_2^{(1-l)/l}(T_0) + L_4}{L_4}\right). \tag{56}$$

where T_0 denotes the initial time.

On the other hand, it follows from (54) that when $V_2 > \left(\frac{\Delta_2}{(1-\Xi_2)L_4}\right)^{l/(2l-1)}$, then $\dot{V}_2 \leq -L^* V_3 - \Xi_2 L_4 V_2^{(2l-1)/l}$. Then, all the system signals converge to the following regions:

$$\begin{cases} \|\tilde{\boldsymbol{\Theta}}\| \leq k_3^{-1}\lambda_{\min}^{-\frac{1}{2}}(\boldsymbol{C})\sqrt{\Omega_4}, & \|\tilde{\boldsymbol{w}}\| \leq \lambda_{\min}^{-\frac{1}{2}}(\boldsymbol{C})\sqrt{\Omega_4}, \\ \|\tilde{\boldsymbol{W}}^*\| \leq \lambda_{\min}^{-\frac{1}{2}}(\boldsymbol{\Upsilon}^{-1})\sqrt{\Omega_4}, & \|\boldsymbol{s}_n\| \leq \sqrt{2}\sqrt{\Omega_4}, \\ |\tilde{r}_{a,i}| \leq \frac{\sqrt{2\sigma}}{\sigma}\sqrt{\Omega_4} \end{cases} \tag{57}$$

where $\Omega_4 = \left(\frac{\Delta_2}{(1-\Xi_2)L_4}\right)^{l/(2l-1)}$. The upper bound of the convergence time T_2 is calculated by

$$T_2 \leq T_0 + \frac{l}{L^*(1-l)}\ln\left(\frac{L^* V_2^{(1-l)/l}(T_0) + \Xi_2 L_4}{\Xi_2 L_4}\right). \tag{58}$$

To sum up, we can know that all the closed-loop signals will converge to the following regions:

$$\begin{cases} \|\tilde{\boldsymbol{\Theta}}\| \leq k_3^{-1}\lambda_{\min}^{-\frac{1}{2}}(\boldsymbol{C})\sqrt{\min\{\Omega_3,\Omega_4\}} \\ \|\tilde{\boldsymbol{w}}\| \leq \lambda_{\min}^{-\frac{1}{2}}(\boldsymbol{C})\sqrt{\min\{\Omega_3,\Omega_4\}} \\ \|\tilde{\boldsymbol{W}}^*\| \leq \lambda_{\min}^{-\frac{1}{2}}(\boldsymbol{\Upsilon}^{-1})\sqrt{\min\{\Omega_3,\Omega_4\}} \\ \|\boldsymbol{s}_n\| \leq \sqrt{2}\sqrt{\min\{\Omega_3,\Omega_4\}} \\ |\tilde{r}_{a,i}| \leq \frac{\sqrt{2\sigma}}{\sigma}\sqrt{\min\{\Omega_3,\Omega_4\}} \end{cases} \tag{59}$$

and the convergence time T_{reach} is bounded by

$$\begin{aligned} T_{\text{reach}} \leq \max\Bigg\{&\frac{l}{\Xi_2 L^*(1-l)}\ln\left(\frac{\Xi_2 L^* V_2^{(1-l)/l}(T_0) + L_4}{L_4}\right) \\ &+ T_0, \frac{l}{L^*(1-l)}\ln\left(\frac{L^* V_2^{(1-l)/l}(T_0) + \Xi_2 L_4}{\Xi_2 L_4}\right) + T_0\Bigg\}. \end{aligned} \tag{60}$$

Next, the error convergence for $\boldsymbol{\Theta}_e$ is studied by transforming (33) into the following form:

$$\begin{aligned}\left(\boldsymbol{\Theta}_e - \frac{\boldsymbol{s}_n}{2}\right) + \left(\beta_a - \frac{\boldsymbol{s}_n}{2}\mathrm{sign}(\boldsymbol{\Theta}_e)^{-m_c}\right)\mathrm{sign}(\boldsymbol{\Theta}_e)^{m_c} \\ + \beta_b \mathrm{sign}(\dot{\boldsymbol{\Theta}}_e)^{m_a/m_b} = 0. \end{aligned} \tag{61}$$

The system states will be maintained in the FNTSM surface if the following conditions are held:

$$2\boldsymbol{\Theta}_e - \boldsymbol{s}_n > 0, \quad 2\beta_a - \boldsymbol{s}_n\mathrm{sign}(\boldsymbol{\Theta}_e)^{-m_c} > 0. \tag{62}$$

From (62), the tracking error $\boldsymbol{\Theta}_e$ converges into the following

$$\|\boldsymbol{\Theta}_e\| \leq \max\left\{\frac{\Lambda}{2}, \left(\frac{\Lambda}{2\beta_a}\right)^{1/m_c}\right\} \tag{63}$$

where $\Lambda = \sqrt{2\min\{\Omega_3,\Omega_4\}}$. The total convergence time T_{total} is $T_{\text{total}} = T_{\text{reach}} + T_{\text{sliding}}$, where T_{reach} has been given earlier, and T_{sliding} is can be computed according to Remark 4 in [31], that is, $T_{\text{sliding}} = \frac{m_a\|\boldsymbol{\Theta}_e(0)\|^{1-\frac{m_b}{m_a}}}{\beta_b(m_a-m_b)} \cdot \Lambda\Big(\frac{m_b}{m_a}, \frac{m_a-m_b}{(m_c-1)m_a}, 1+\frac{m_a-m_b}{(m_c-1)m_a}, -\beta_a\|\boldsymbol{\Theta}_e(0)\|^{m_c-1}\Big)$. By using $\left(1+\frac{m_a-m_b}{(m_c-1)m_a}\right) - \frac{m_a-m_b}{(m_c-1)m_a} - \frac{m_b}{m_a} = 1 - \frac{m_b}{m_a} \in \left(0, \frac{1}{2}\right)$ and $-\beta_a\|\boldsymbol{\Theta}_e(0)\|^{m_c-1} < 0$ and Lemma 4, it follows that the function $\Lambda(\cdot)$ is convergent. Thus, Theorem 2 is proved.

Remark 5: In (41), $\boldsymbol{u}_{o,eq}$ is the equivalent control signal to drive the system states into the sliding mode surface under the ideal conditions, $\boldsymbol{u}_{o,sw,1}$ is designed to realize the fast finite-time convergence and alleviate the undesired chattering, $\boldsymbol{u}_{o,sw,2}$ is the fuzzy control signal to stem from the time-varying external disturbances, uncertain parameters and actuator faults, and $\boldsymbol{u}_{o,sa}$ is the saturation compensation control law to restrain the negative effects of the input saturation.

Remark 6: For the auxiliary system in (38) and (39), there are two advantages to be pointed out: (1) Different from [44], the singularity problem can be effectively avoided in this study when the state $\boldsymbol{\xi}$ closes to zero. (2) Unlike [45], this study designs an auxiliary system without the boundedness information of $\Delta\boldsymbol{u}$. (3) Compared with [46], the output of the auxiliary system is smooth. These help improve the anti-saturation ability and release the application limitation.

Remark 7: In contrast to the well-known conclusions on adaptive fuzzy control approaches, the main differences of this study are described as follows:

1) The system states in [17], [18] are supposed to be known, and our results are derived without requiring the system states to be known.
2) The control performance in [17], [21], [22], [46] can be achieved when the convergence time is infinite, while our work can achieve the control objective when the convergence time is finite.
3) The control framework of adaptive fuzzy control has a simpler fuzzy structure and fewer fuzzy gains to handle the lumped disturbance compared to the existing works on the attitude control of the quadrotor UAV [3], [15], [17], which helps to reduce the computational burden of fuzzy approximation.

Remark 8: To achieve better attitude control performance, the main design parameters should be carefully selected according to the following criteria:

1) *Choice of parameters m_i and l_j, $(i = a, b, c; j = 1, 2)$:* Under the conditions $1 < \frac{m_a}{m_b} < 2$ and $m_c > \frac{m_a}{m_b}$, larger values $\frac{m_a}{m_b}$ and m_c can improve the convergence speed. From (30) and $\frac{4}{5} < l < 1$, a smaller value l is useful for providing high-accuracy state estimation, but in turn, it tends to cause high-frequency oscillations. Moreover, positive odd integers l_1 and l_2 are chosen based on $2l - 1 = \frac{l_1}{l_2}$.
2) *Choice of parameters β_i and n_i, $(i = a, b)$:* In order to realize shorter convergence time and smaller convergence regions, large values β_a and β_b are usually selected. A larger value $n_a > 1$ can quickly overcome the effect of the saturation error, while the parameter $n_b > 0$ plays a key role in achieving the finite-time convergence property.
3) *Choice of parameters σ and μ_i, $(i = 1, 2, 3)$:* The parameter σ is introduced to adjust the update rate of $\hat{\boldsymbol{r}}_a$, which is usually chosen to be small enough to accelerate the update speed, but it may cause the overestimation problem. Besides, an appropriate value μ_i can guarantee the finite-time convergence and avert the drift of the parameter $\hat{\boldsymbol{r}}_a$.
4) *Choice of parameters k_i, $(i = a, b, c, d)$:* Since this study designs an adaptive fuzzy control part, the values of the control gains k_a and k_b can be selected to be smaller than the work [10], which helps to reduce the input amplitude. The term $\text{sign}(\boldsymbol{s}_n)^{\frac{k_c}{k_d}}$ with $k_c < k_d$ can enhance the system robustness, where a larger value $\frac{k_c}{k_d}$ helps reduce the chattering phenomenon but decreases the system robustness. Thus, it should make a balance in the choice of the value $\frac{k_c}{k_d}$.

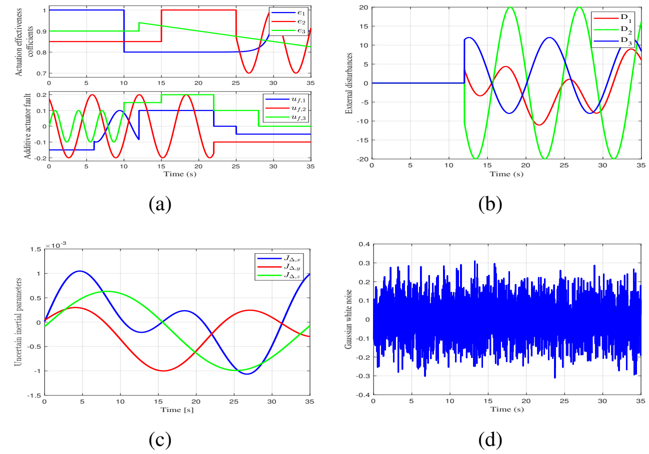

Fig. 5. *Simulation:* Time response of various disturbance factors. (a) Actuation effectiveness factor and additive actuator fault, (b) External disturbances, (c) Parametric uncertainties, (d) Gaussian white noise.

In particular, there is no standard procedure for selecting these design parameters. They are currently chosen by trial and error until satisfactory control results are achieved.

IV. Simulations and Experiments

In addition to the aforementioned theoretical discussion and analysis, extensive simulations and experiments are performed in this section to verify the validity of the proposed controller, by comparing the proposed controller without an auxiliary system, proportion-differentiation (PD), finite-time DSC [18], DO–NTSMC [35], adaptive fuzzy finite-time control [22], FTC–NFTSM [33], and adaptive NFTSMC [34]. The comparison of the proposed controller, the proposed controller without an auxiliary system, PD, finite-time DSC [18], DO–NTSMC [35] and adaptive fuzzy finite-time control [16] is to verify that the proposed controller can achieve saturation elimination, fault tolerance, and strong robustness, while the comparison of the proposed controller without an auxiliary system, FTC–NFTSM [33], and adaptive NFTSMC [34] is to verify that the proposed switching control part is capable of realizing free chattering. With the help of the auxiliary system, only the proposed controller can solve the input saturation.

A. Simulation analysis

Simulation: The reference attitude command $\boldsymbol{\Theta}_d(t) = [\phi_d(t); \theta_d(t); \varphi_d(t)]$ is predefined by

$$\phi_d(t) = 1, \quad \theta_d(t) = t/35,$$

$$\varphi_d(t) = \begin{cases} 1, & \text{if} \quad 0 < t \leq 10 \\ 0.5, & \text{if} \quad 10 < t \leq 25 \\ 0, & \text{if} \quad 25 < t \leq 35 \end{cases},$$

and the initial states of the actual attitudes are randomly selected as $[\phi(0); \theta(0); \varphi(0)] = [0; 1; 0]$ [rad]. The physical parameters are set as $m = 2$ [kg], $l_d = 0.2$ [m], $J_{0,x} = J_{0,y} =$

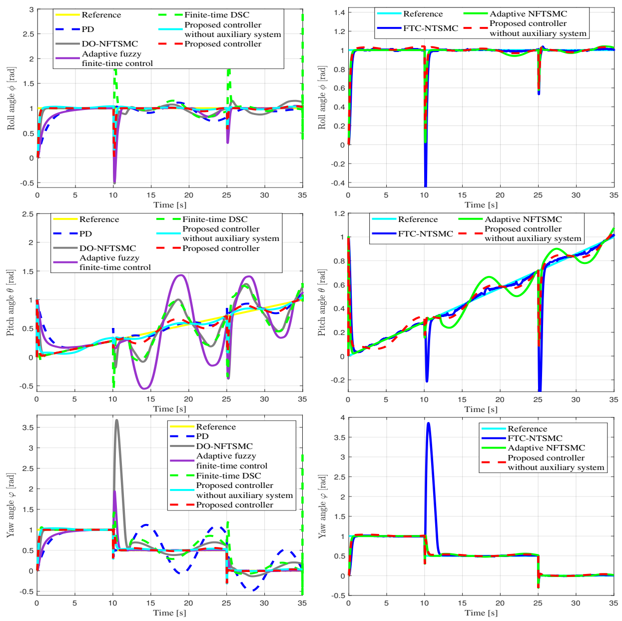

Fig. 6. *Simulation:* Time response of attitude signals.

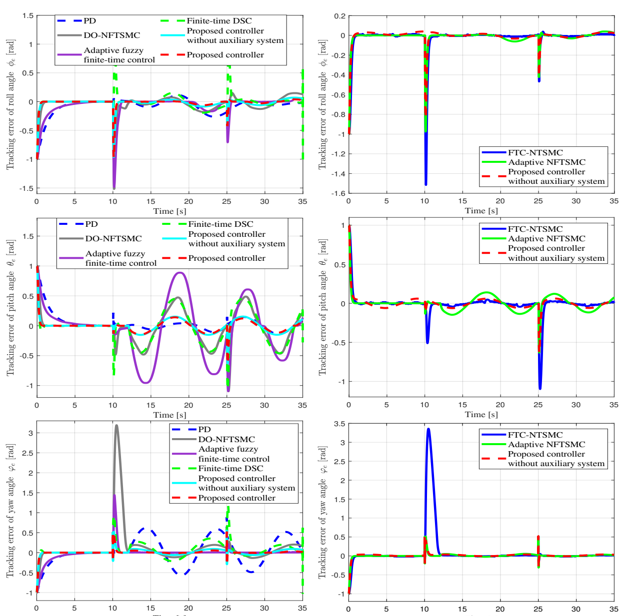

Fig. 7. *Simulation:* Time response of attitude errors.

$0.01175~[\mathrm{N\cdot m\cdot s^2/rad}]$, and $J_{0,z} = 0.02229~[\mathrm{N\cdot m\cdot s^2/rad}]$. The signals of external disturbances, uncertain parameters, actuator faults, and Gaussian white noise with 0.1 level are added to illustrate noise immunity and controller robustness, as shown in Fig. 5. The control parameters are set as $\boldsymbol{m}_r = [m_{1,r}; m_{2,r}; m_{1,3}] = [1.2; 1.2; 1.2]$, $\boldsymbol{m}_l = [m_{1,l}; m_{2,l}; m_{3,l}] = [-1.2; -1.2; -1.2]$, $\sigma = 0.05$, $\mu_1 = \mu_2 = 0.0015$, $\mu_3 = 0.002$, $\hat{\boldsymbol{r}}_a(0) = [\hat{r}_{a,1}(0); \hat{r}_{a,2}(0); \hat{r}_{a,3}(0)] = [0.01; 0.01; 0.01]$, $m_a = 19$, $m_b = 17$, $m_c = 1.1$, $k_a = k_b = 18$, $k_c = 13$, $k_d = 20$, $\beta_a = 3$, $\beta_b = 0.1$, $n_a = 15$, $n_b = 10$, $l = \frac{8}{9}$, $k_1 = 0.01$, $k_2 = 0.02$, $k_3 = 0.2$, $k_4 = 0.1$, $p = 15$, $\kappa_i = 2$, $\boldsymbol{C}_i$ is evenly distributed in the interval $[-2, 2]$, $\boldsymbol{\Upsilon} = 10\boldsymbol{I}_{3\times 3}$, $\hat{\boldsymbol{w}}(0) = 0$, $\hat{\boldsymbol{W}}^*(0) = 0$, $\hat{\boldsymbol{\Theta}}(0) = 0$, and $\boldsymbol{\chi}(0) = 0$. The fuzzy

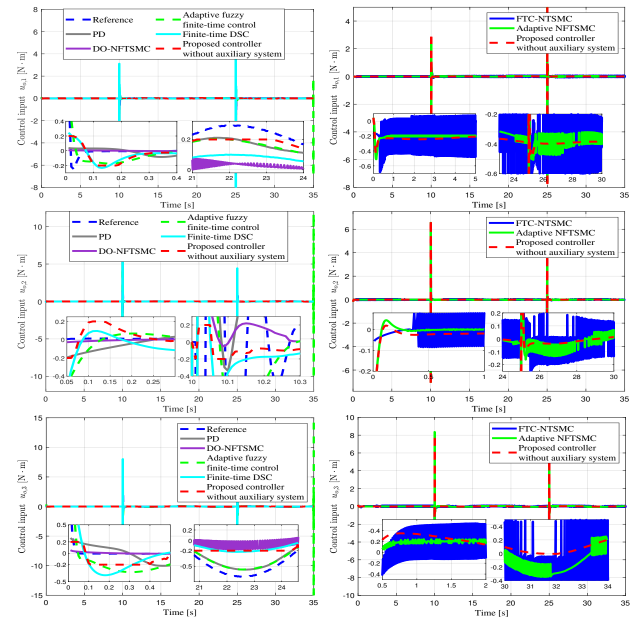

Fig. 8. *Simulation:* Time response of control inputs.

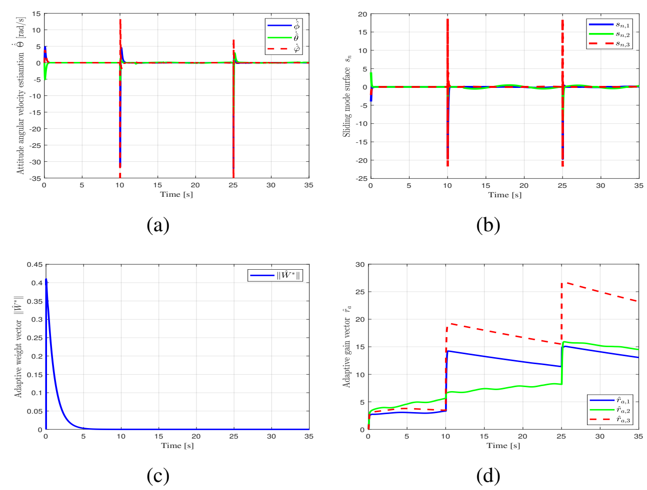

Fig. 9. *Simulation:* Time response of various system states under the proposed controller. (a) Estimation of the attitude angular velocity based on the designed AFTNNO, (b) NFTSM surface, (c) Adaptive RBFNN weight, (d) Adaptive fuzzy gains.

rules are set as follows: if $s_{n,i} > 1.2$, than $v_{i,1} = 1$, $v_{i,2} = 0$ and $v_{i,3} = 0$; if $0 < s_{n,i} \leq 1.2$, than $v_{i,1} = 0.5$, $v_{i,2} = 0.5$ and $v_{i,3} = 0$; if $-1.2 < s_{n,i} \leq 0$, than $v_{i,1} = 0$, $v_{i,2} = 0.5$ and $v_{i,3} = 0.5$; else if $s_{n,i} \leq -1.2$, than $v_{i,1} = 0$, $v_{i,2} = 0$ and $v_{i,3} = 1$, where $i = 1, 2, 3$. The input saturation $\mathrm{sat}(u_{o,i})$ is described as

$$\mathrm{sat}\big(u_{o,i}(t)\big) = \begin{cases} -0.2, & u_{o,i}(t) < -0.2 \\ u_{o,i}(t), & -0.2 \leq u_{o,i}(t) \leq 0.2 \\ 0.2, & u_{0,i}(t) > 0.2 \end{cases}.$$

The control results of comparative simulations are visually shown in Fig. 6 to Fig. 9. As depicted in Fig. 6, we can see that the proposed controllers with/without an auxiliary system can resume to closely track the desired attitude signals after a short transient period even if larger disturbances suddenly happen, and have smaller oscillations than other controllers. It

Fig. 10. Quadrotor platform used in the experiments

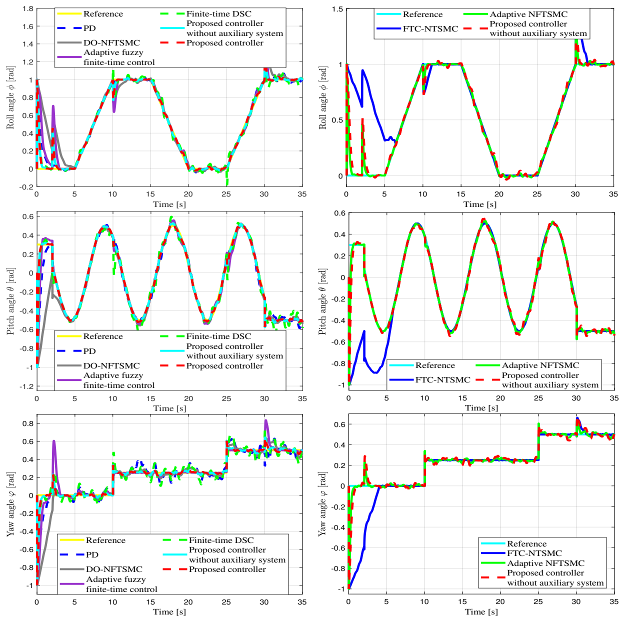

Fig. 11. *Experiment 1:* Time response of attitude signals.

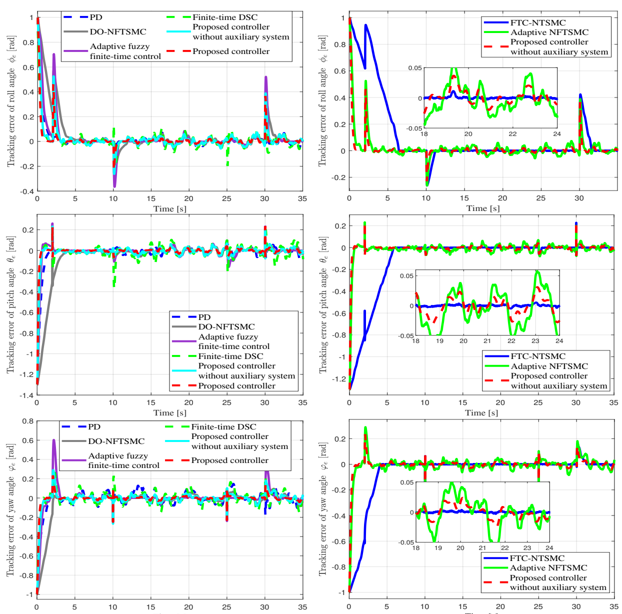

Fig. 12. *Experiment 1:* Time response of attitude errors.

should be noticed that although other comparative controllers also have the ability to stabilize the attitude system and achieve acceptable attitude control performance when the disturbances do not increase, the output attitude signals are difficult to accurately track the desired signals when the disturbances become suddenly large at the time $t = 10$ [s]. These results

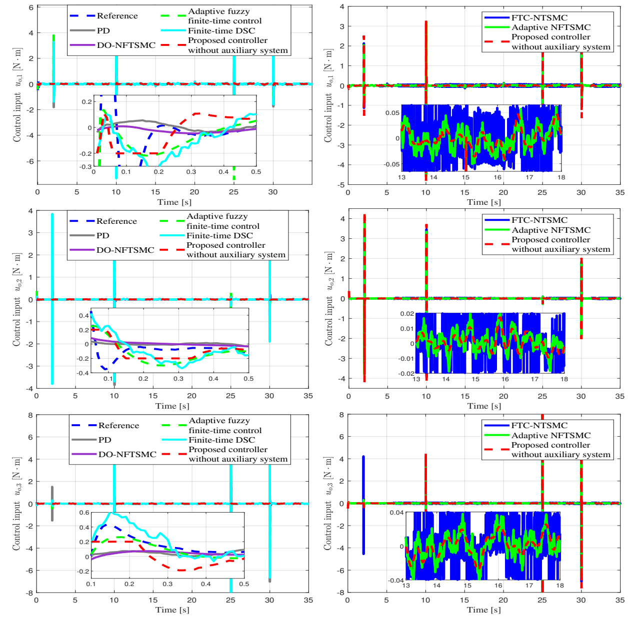

Fig. 13. *Experiment 1:* Time response of control inputs.

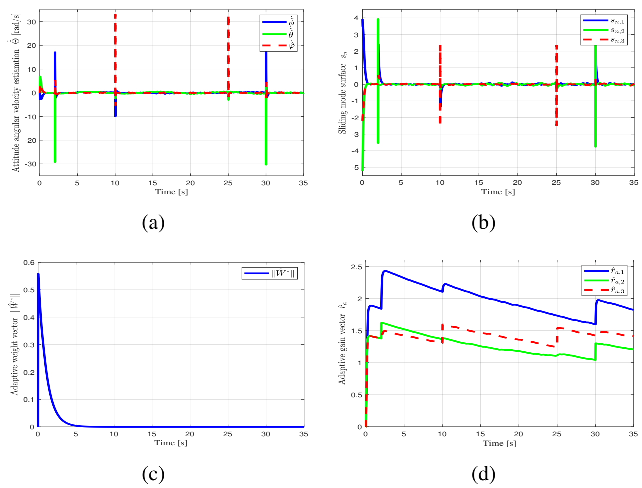

Fig. 14. *Experiment 1:* Time response of various states under the proposed controller. (a) Estimation of the attitude angular velocity based on the designed AFTNNO, (b) NFTSM surface, (c) Adaptive RBFNN weight, (d) Adaptive fuzzy gains.

reflect that the proposed controllers with/without an auxiliary system can improve the ability of disturbance suppression. To be precise, it can be found from Fig. 7 that the tracking errors of the proposed controllers with/without an auxiliary system are smaller than those of other remaining controllers, which fully illustrates that the proposed controllers with/without an auxiliary system are obviously less affected by system uncertainties, time-varying disturbances, and actuator faults. From Fig. 8, the time responses of control inputs infer that the proposed controller can effectively overcome the input saturation and is protected from the chattering influence, while the FTC-NTSMC and adaptive NFTSMC methods suffer from serious chattering issues and the DO-NFTSMC method has a slightly chattering phenomena. This reason is that the switching control part $\boldsymbol{u}_{o,sw}$ in (37) containing the fast-type control $u_{o,sw,1}$ and

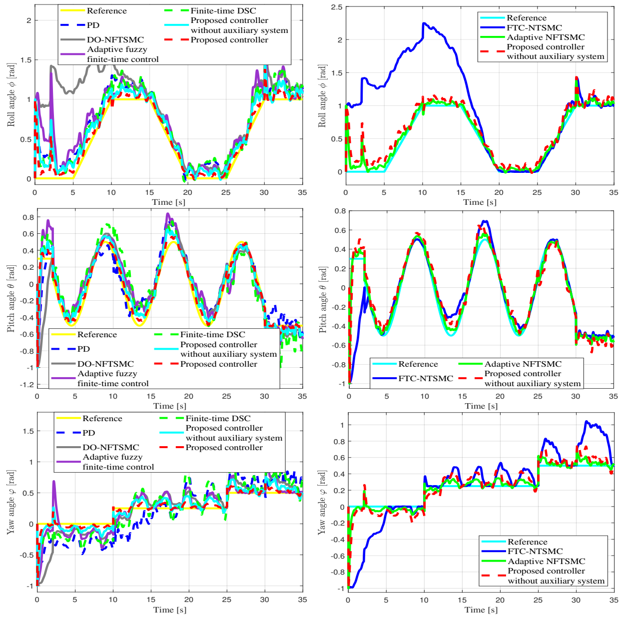

Fig. 15. *Experiment 2:* Time response of attitude signals.

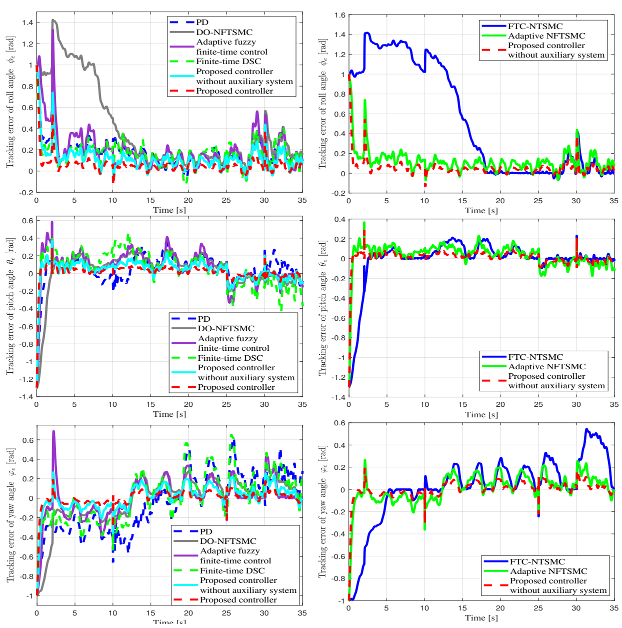

Fig. 16. *Experiment 2:* Time response of attitude errors.

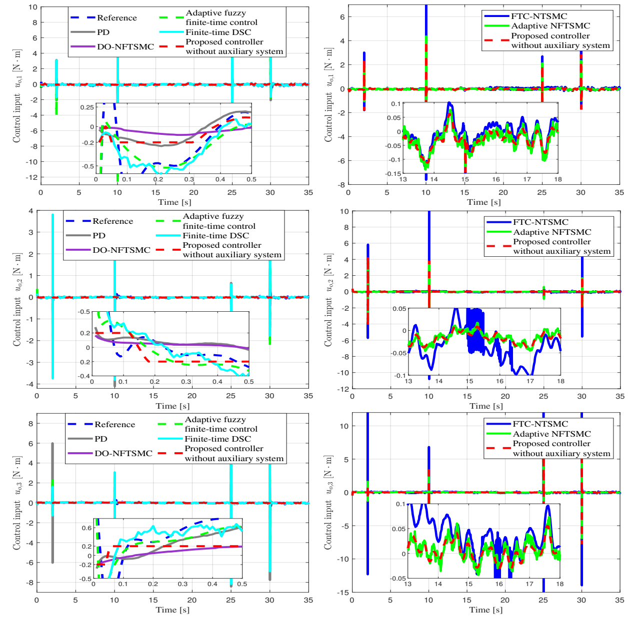

Fig. 17. *Experiment 2:* Time response of control inputs.

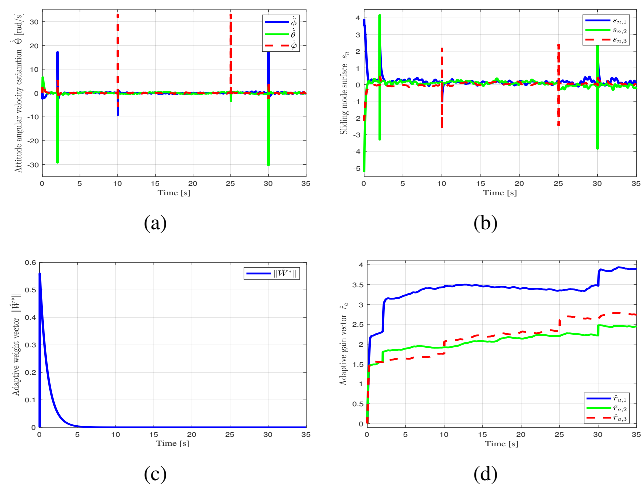

Fig. 18. *Experiment 2:* Time response of various states under the proposed controller. (a) Estimation of the attitude angular velocity based on the designed AFTNNO, (b) NFTSM surface, (c) Adaptive RBFNN weight, (d) Adaptive fuzzy gains.

the compensation control $u_{o,sw,2}$ can reduce control gain and accelerate the convergence rate. As shown in Fig. 9 (a), it can be observed that the designed AFTNNO can realize the precise estimation of theangular velocity even in the presence of the lumped disturbance and input saturation. Figs. 9 (b) and (c) show the time responses of sliding mode surfaces and the norm of adaptive RBFNN weight, respectively. In addition, Fig. 9 (d) displays the evolution of adaptive fuzzy gain, and we can see that there is no parameter drift problem.

B. Experiment analysis

To better demonstrate the superiority of the proposed controller, comparative experiments are performed in this subsection. The hardware configuration of the quadrotor UAV is shown in Fig. 10, where the personal computer is used to detect the quadrotor's states, a digital signal processor is utilized as the on-board control computer to execute the control algorithm, the attitude information can be estimated by an inertial measurement unit, the desired attitude signals are generated by a remote controller, and the wireless data transmission module is used to establish the network communication between the quadrotor UAV, the remote controller, and the ground station. The motor speed signals are sent from the on-board control computer to four electronic speed controllers by a serial peripheral interface bus.

Experiment 1: Consider the external disturbances and input saturation during the entire flight duration. The desired com-

TABLE I
COMPARISON OF ATTITUDE CONTROL PERFORMANCE

Mode	Index	Unit	Value							
			Proposed controller	Proposed controller without auxiliary system	PD	Finite-time DSC [18]	DO–NTSMC [35]	Adaptive fuzzy finite-time control [22]	FTC–NFTSMC [33]	Adaptive NFTSMC [34]
Simulation	μ_{SE}	rad^2	82.25	81.91	607.25	485.11	1201.22	1026.55	901.95	108.9
	μ_{AE}	rad	364.01	362.25	1556.82	1375.15	1567.31	1668.45	614.95	385.69
	μ_{TWAE}	$\mathrm{rad \cdot s}$	189.59	188.71	784.73	830.88	841.82	805.39	206.85	380.38
	μ_{TEC}	$\mathrm{N \cdot m}$	572.58	1504.65	1483.65	2507.41	1336.65	1757.17	2559.21	1104.6
Experiment 1	μ_{SE}	rad^2	58.1	56.7	112.69	87.15	353.53	156.45	753.18	89.25
	μ_{AE}	rad	192.85	188.32	455.73	504.35	728.68	365.43	1036.35	325.85
	μ_{TWAE}	$\mathrm{rad \cdot s}$	63.75	62.17	165.33	229.22	165.89	91.54	106.35	117.51
	μ_{TEC}	$\mathrm{N \cdot m}$	422.08	1081.52	721.73	807.81	965.65	1101.79	1724.45	985.25
Experiment 2	μ_{SE}	rad^2	86.5	84.21	568.05	491.41	1509.55	443.19	2563.42	213.49
	μ_{AE}	rad	532.04	514.85	1961.41	1873.89	2609.57	1622.60	3075.28	1059.45
	μ_{TWAE}	$\mathrm{rad \cdot s}$	215.96	208.94	850.79	872.79	873.93	609.51	840.78	447.90
	μ_{TEC}	$\mathrm{N \cdot m}$	468.87	1959.65	2058.00	1724.45	1895.25	1904.01	3313.3	1928.15

mand $\boldsymbol{\Theta}_d(t) = [\phi_d(t); \theta_d(t); \varphi_d(t)]$ is predefined as follows:

$$\phi_d(t) = \begin{cases} 0 & \text{if} \quad 0 < t \le 5 \\ 0.2t - 1 & \text{if} \quad 5 < t \le 10 \\ 1 & \text{if} \quad 10 < t \le 15 \\ -0.2t + 4 & \text{if} \quad 15 < t \le 20 \\ 0 & \text{if} \quad 20 < t \le 25 \\ 0.2t - 5 & \text{if} \quad 25 < t \le 30 \\ 1 & \text{if} \quad 30 < t \le 35 \end{cases},$$

$$\theta_d(t) = \begin{cases} 0.3 & \text{if} \quad 0 < t \le 2 \\ 0.5\cos(0.7t) & \text{if} \quad 2 < t \le 30 \\ -0.5 & \text{if} \quad 30 < t \le 35 \end{cases},$$

$$\varphi_d(t) = \begin{cases} 0 & \text{if} \quad 0 < t \le 10 \\ 0.25 & \text{if} \quad 10 < t \le 25 \\ 0.5 & \text{if} \quad 25 < t \le 35 \end{cases}.$$

The control parameters are set as $\boldsymbol{m}_r = [m_{1,r}; m_{2,r}; m_{3,r}] = [1.5; 1.5; 1.5]$, $\boldsymbol{m}_l = [m_{1,l}; m_{2,l}; m_{3,l}] = [-1.5; -1.5; -1.5]$, $\sigma = 0.1$, $\mu_1 = \mu_2 = 0.005$, $\mu_3 = 0.002$, $\hat{\boldsymbol{r}}_a(0) = [\hat{r}_{a,1}(0); \hat{r}_{a,2}(0); \hat{r}_{a,3}(0)] = [0.01; 0.01; 0.01]$, $m_a = 23$, $m_b = 21$, $m_c = 1.1$, $k_a = k_b = 25$, $k_c = 25$, $k_d = 17$, $\beta_a = 2$, $\beta_b = 0.3$, $n_a = 15$, $n_b = 10$, $l = \frac{8}{9}$, $k_1 = 0.01$, $k_2 = 0.01$, $k_3 = 0.3$, $k_4 = 0.2$, $p = 25$, $\kappa_i = 1.5$, $\boldsymbol{C}_i$ is evenly distributed in the interval $[-2.5, 2.5]$, $\boldsymbol{\Upsilon} = 12\boldsymbol{I}_{3\times 3}$, $\hat{\boldsymbol{w}}(0) = 0$, $\hat{\boldsymbol{W}}^*(0) = 0$, $\hat{\boldsymbol{\Theta}}(0) = 0$, and $\boldsymbol{\chi}(0) = 0$. The fuzzy rules are set as follows: if $s_{n,i} > 1.5$, than $v_{i,1} = 1$, $v_{i,2} = 0$ and $v_{i,3} = 0$; if $0 < s_{n,i} \le 1.5$, than $v_{i,1} = 0.5$, $v_{i,2} = 0.5$ and $v_{i,3} = 0$; if $-1.5 < s_{n,i} \le 0$, than $v_{i,1} = 0$, $v_{i,2} = 0.5$ and $v_{i,3} = 0.5$; else if $s_{n,i} \le -1.5$, than $v_{i,1} = 0$, $v_{i,2} = 0$ and $v_{i,3} = 1$, where $i = 1, 2, 3$.

The obtained results of the *Experiment 1* are depicted in Figs. 11 to 14. Figs. 11 and 12 display the tracking performance of attitude angles and the change of the attitude tracking errors with time, respectively. One can see from Fig. 11 and 12 that the proposed controllers with/without an auxiliary system *not only* overcome the effect of the disturbances in a short time *but also* avert large oscillations during the control process. In particular, the curves of the proposed controllers with/without an auxiliary system are almost the same. These visually exhibit satisfactory robustness of the proposed controller even in the presence of input saturation. From the three sub-figures on the left side of Fig. 13, with the help of the designed auxiliary system, the control inputs of the proposed controller are constrained within the specified range. To avoid the interference of the auxiliary system, we compare with the proposed controller, FTC-NTSMC and adaptive NFTSMC to infer that the chattering issue can be solved, as depicted in the three sub-figures on the right of Fig. 13. From Fig. 14 (a), the designed AFTNNO can estimate the information of angular velocities accurately. Figs. 14 (b)–(c) show the curves of the sliding mode surfaces and the norm of the RBFNN weight, respectively. The time evolution of the adaptive fuzzy gains is shown in Fig. 9 (d), which indicates that the problem of the parameter drifting can be avoided. The control performance of the *Experiment 1* is consistent with the theoretical analysis and simulation results.

Experiment 2: Based on the *Experiment 1*, the *Experiment 2* considers stronger disturbances and persistent actuator faults. Apart from this, other conditions such as the desired attitude signal and control parameters are the same as the *Experiment 1*. The effectiveness matrix $\boldsymbol{E}$ and additive actuator fault $\boldsymbol{u}_f$ are set as $\boldsymbol{E} = \mathrm{diag}\{0.85 + 0.15\sin(0.5t); 0.9 + 0.1\cos(t); 0.75 + 0.25\cos(1.2t)\}$ and $\boldsymbol{u}_f = [3 - \cos(2t); 2 + \sin(0.5t); 2\cos(t)]$, respectively. In the experimental tests, the actuator faults are injected by software via the thrust signals before being sent to the quadrotor UAV.

The comparative results of the *Experiment 2* are shown in Figs. 15 to 18. The real attitude signals of different controllers and the corresponding tracking errors are depicted in Figs. 15 and 16, respectively. From Figs. 15 and 16, one can find that although the quadrotor UAV is subjected to bigger disturbances, persistent actuator faults, and input saturation, the proposed controller still makes the real attitude signals rapidly return to the desired attitude signals and maintains satisfactory tracking effects. These imply that the proposed controller is almost unaffected by the above negative factors, and has stronger system robustness than other controllers. As shown in Fig. 17, it can be seen that the control inputs of the proposed controller are still within the prescribed range even when the saturation issue occurs in comparison to the proposed controller without an auxiliary system, and the proposed

TABLE II
CHANGE OF PERFORMANCE INDICES IN EXPERIMENT 2 TO EXPERIMENT 1

Index	Value (Unit: %)							
	Proposed controller	Proposed controller without auxiliary system	PD	Finite-time DSC [18]	DO–NTSMC [35]	Adaptive fuzzy finite-time control [22]	FTC–NFTSMC [33]	Adaptive NFTSMC [34]
μ_{SE}	48.88	48.52	80.16	82.27	76.58	71.20	70.62	58.20
μ_{AE}	63.75	63.42	76.78	73.09	77.08	77.48	66.30	352.44
μ_{TWAE}	70.48	70.24	83.15	73.74	81.02	84.98	87.35	73.76
μ_{TEC}	82.16	81.24	92.71	127.01	96.27	72.81	92.14	95.70

controller can avoid the chattering issue in comparison to the FTC-NTSMC and adaptive NFTSMC. The control results in terms of the fault tolerance, saturation elimination, and free chattering are attributed to the adaptive fuzzy mechanism and the auxiliary system. Fig. 18(a) shows that the AFTNNO can precisely estimate the information of angular velocity online. As shown in Fig. 18 (b), the dynamics of the sliding mode surface $\boldsymbol{s}_n$ can be quickly stabilized around zero. Besides, the time responses of the adaptive RBFNN weight $\|\hat{W}^*\|$ and the adaptive fuzzy gain $\hat{r}_a$ are clearly shown in Figs. 18 (c) and (d), respectively, which means that the designed adaptive parameters would ultimately converge.

C. Numerical analysis

To quantitatively evaluate the performance of different controllers, four performance indices [49] are employed in this study and are concretely described as 1) Squared error (SE): $\mu_{SE} = \sum_{i=1}^{N}\big(\phi_e^2(i) + \theta_e^2(i) + \varphi_e^2(i)\big)[\mathrm{rad}^2]$; 2) Absolute error (AE): $\mu_{AE} = \sum_{i=1}^{N}\big(|\phi_e(i)| + |\theta_e(i)| + |\varphi_e(i)|\big)[\mathrm{rad}]$; 3) Time-weighted absolute error (TWAE): $\mu_{TAE} = \frac{1}{N}\sum_{i=1}^{N} i\big(|\phi_e|(i) + |\theta_e(i)| + |\varphi_e(i)|\big)[\mathrm{rad}\cdot\mathrm{s}]$; 4) Total energy consumption (TEC): $\mu_{TEC} = \sum_{i=1}^{N}\big(|u_1(i)| + |u_2(i)| + |u_3(i)|\big)[\mathrm{N}\cdot\mathrm{m}]$, where N is the total time of the simulation operation. Since the tracking errors and control inputs may be negative, these indices are mostly described by using either the absolute value or the square value. Especially, the smaller values of μ_{SE}, μ_{AE}, μ_{TWAE} and μ_{TEC} illustrate less persistent oscillations, quicker convergence rate, higher steady-state precision, and less energy consumption, respectively.

The values of the above performance indices are recorded in Tables I and II to better explain the superiority of the proposed controller. From Table I, it can be seen that all the index values of the proposed controllers with/without an auxiliary system are smaller than those of the other six controllers, which strongly implies that the proposed control framework can provide a higher precision. By comparing the proposed controller and adaptive NFTSMC, it can be illustrated that the adaptive fuzzy control part can improve the robustness of the system to various disturbances. In contrast to the proposed controller without an auxiliary system, the proposed controller successfully addresses the problem of input saturation with the help of the designed auxiliary system. Actually, the input saturation limits the growth of the control input, which inevitably leads to slower tracking speed. However, the control precision is slightly reduced, but not significantly. The reason for this is that the designed auxiliary system could limit the control input beyond the specified requirements. In addition, one can see from Table II that when external disturbances become larger and the actuator faults occur, the proposed controllers with/without an auxiliary system are much less affected than the other controllers when the control parameters are not reset, which means that the proposed control framework has higher adaptability and stronger robustness. Through experimental implementation and numerical analysis, it fully demonstrates the feasibility and superiority of the proposed controller in terms of disturbance suppression, free-chattering, fault tolerance, and saturation elimination.

V. CONCLUSION

This study designs an observer-based adaptive fuzzy finite-time attitude control strategy for quadrotor UAVs under unavailable angular velocity, external disturbances, uncertain dynamics, actuator faults, and input saturation. First, an AFTNNO is constructed to estimate the information of angular velocity online. Subsequently, an adaptive FLS-based NFTSMC scheme is proposed to automatically adjust the control gain. Furthermore, an auxiliary system with free singularity is designed to overcome the input saturation. Although a series of comparative simulations and real-time experiments authenticate the advantages and effectiveness of the proposed control strategy, the following limitations are worth to be investigated in the future: 1) Although the Remark 8 gives detailed guidance on how to choose the control parameters, it is necessary to study the reliable tuning mechanism so as to obtain their optimal values; 2) Although the designed FLS provides a simpler fuzzy structure and fewer logic rules, the design complexity of the whole control system has not significantly reduced, which is one of the future studies; and 3) Since the problems of sensor failures and state constraints are not considered, our research direction will also focus on how to ensure the safer flight in the ever-changing environments.

REFERENCES

[1] G. V. Raffo, M. G. Ortegam, and F. R. Rubio, "An integral predictive/nonlinear $\mathcal{H}_\infty$ control structure for a quadrotor helicopter," *Automatica*, vol. 46, pp. 29-39, 2010.

[2] H. Hua, Y. Fang, X. Zhang, and B. Lu, "A novel robust observer-based nonlinear trajectory tracking control strategy for quadrotors," *IEEE Trans. Control Syst. Technol.*, vol. 29, no. 5, pp. 1952–1963, Sept. 2021.

[3] Q. Chen, M. Tao, X. He, and L. Tao, "Fuzzy adaptive nonsingular fixed-time attitude tracking control of quadrotor UAVs," *IEEE Trans. Aerosp. Electron. Syst.*, vol. 57, no. 5, pp. 2864-2877, Oct. 2021.

[4] K. Liu and R. Wang, "Antisaturation adaptive fixed-time sliding mode controller design to achieve faster convergence rate and its application", *IEEE Trans. Circuits Syst. II, Exp. Briefs*, vol. 69, no. 8, pp. 3555-3559, Aug. 2022.

[5] K. Liu, R. Wang, X. Wang, and X. Wang, "Antisaturation adaptive finite-time neural network based fault-tolerant tracking control for a quadrotor UAV with external disturbances", *Aerosp. Sci. Technol.*, vol. 115, pp. 106790, Aug. 2021.

[6] M. Sharma and I. Kar, "Control of a quadrotor with network induced time delay," *ISA Trans.*, vol. 111, pp. 132–143, 2021.

[7] J. Jia, K. Guo, X. Yu, L. Guo, and L. Xie, "Agile flight control under multiple disturbances for quadrotor: Algorithms and evaluation," *IEEE Trans. Aerosp. Electron. Syst.*, vol. 58, no. 4, pp. 3049–3062, Aug. 2022.

[8] M. Labbadi and M. Cherkaoui, "Adaptive fractional-order nonsingular fast terminal sliding mode based robust tracking control of quadrotor UAV with gaussian random disturbances and uncertainties," *IEEE Trans. Aerosp. Electron. Syst.*, vol. 57, no. 4, pp. 2265-2277, Aug. 2021.

[9] S. Lian, W. Meng, Z. Lin, K. Shao, J. Zheng, H. Li, and R. Lu, "Adaptive attitude control of a quadrotor using fast nonsingular terminal sliding mode," *IEEE Trans. Ind. Electron.*, vol. 69, no. 2, pp. 1597–1607, Feb. 2022.

[10] L. Zhang, L. Liu, Z. Wang, and Y. Xia, "Continuous finite-time control for uncertain robot manipulators with integral sliding mode," *IET Contr. Theory Appl.*, vol. 12, no. 11, pp. 1621–1627, Jul. 2018.

[11] Y. Song, L. He, D. Zhang, and J. Qian, "Neuroadaptive fault-tolerant control of quadrotor UAVs: A more affordable solution," *IEEE Trans. Neural Netw. Learn. Syst.*,, vol. 30, no. 7, pp. 1975–1983, Jul. 2019.

[12] X. Zhang, Y. Wang, G. Zhu, X. Chen, and C. -Y. Su, "Discrete-time adaptive neural tracking control and its experiments for quadrotor unmanned aerial vehicle systems," *IEEE/ASME Trans. Mechatronics*, vol. 28, no. 3, pp. 1201–1212, June 2023.

[13] V. K. Tripathi, S. C. Yogi, A. K. Kamath, L. Behera, N. K. Verma, and S. Nahavandi, "A disturbance observer-based intelligent finite-time sliding mode flight controller design for an autonomous quadrotor," *IEEE Syst. J.*, vol. 16, no. 1, pp. 780–790, Mar. 2022.

[14] C. Qian, Y. Fang, and Y. Li, "Neural network-based hybrid three-dimensional position control for a flapping wing aerial vehicle," *IEEE Trans. Cybern*, to be published, DOI: 10.1109/TCYB.2022.3166566.

[15] S. J. Haddadi, P. Zarafshan, and M. Dehghani, "A coaxial quadrotor flying robot: Design, analysis and control implementation", *Aerosp. Sci. Technol.*, vol. 120, pp. 107260, 2022.

[16] Y. Liu, H. Zhang, Y. Wang, H. Ren, and Q. Li, "Adaptive fuzzy prescribed finite-time tracking control for nonlinear system with unknown control directions," *IEEE Trans. Fuzzy Syst.*, vol. 30, no. 6, pp. 1993–2003, June 2022.

[17] C. Li, Y. Wang, and X. Yang, "Adaptive fuzzy control of a quadrotor using disturbance observer", *Aerosp. Sci. Technol.*, vol. 128, pp. 107784, 2022.

[18] H. Wang, K. Xu, P. X. Liu, and J. Qiao, "Adaptive fuzzy fast finite-time dynamic surface tracking control for nonlinear systems," *IEEE Trans. Circuits Syst. I, Reg. Papers*, vol. 68, no. 10, pp. 4337–4348, Oct. 2021.

[19] A. Li, C. K. Ahn, and M. Liu, "T-S fuzzy-based event-triggering attitude-tracking control for elastic spacecraft with quantization," *IEEE Trans. Aerosp. Electron. Syst.*, vol. 58, no. 1, pp. 124–139, Feb. 2022.

[20] X. Ma, M. Chen, G. Feng, and Q. WU, "19," *IEEE Trans. Fuzzy Syst.*, vol. 31, no. 1, pp. 184–198, Jan. 2023.

[21] L. Sun and J. Jiang, "Robust hierarchical adaptive fuzzy relative motion coordination for feature points of two rigid bodies with input and output constraints," *IEEE Trans. Fuzzy Syst.*, vol. 30, no. 2, pp. 475–485, Feb. 2022.

[22] M. Van and S. S. Ge, "Adaptive fuzzy integral sliding mode control for robust fault tolerant control of robot manipulators with disturbance observer," *IEEE Trans. Fuzzy Syst*, vol. 29, no. 5, pp. 1284–1296, May 2021.

[23] F. Wang, H. Gao, K. Wang, C. Zhou, Q. Zong, and C. Hua, "Disturbance observer-based finite-time control design for a quadrotor UAV with external disturbance," *IEEE Trans. Aerosp. Electron. Syst.*, vol. 57, no. 2, pp. 834–847, Apr. 2021.

[24] K. Eliker and W. Zhang, "Finite-time adaptive integral backstepping fast terminal sliding mode control application on quadrotor UAV," *Int. J. Control Autom. Syst.*, vol. 18, no. 2, pp. 415–430, Feb. 2020.

[25] V. K. Tripathi, A. K. Kamath, L. Behera, N. K. Verma, and S. Nahavandi, "An adaptive fast terminal sliding-mode controller with power rate proportional reaching law for quadrotor position and altitude tracking," *IEEE Trans. Syst., Man, Cybern., Syst.*, vol. 52, no. 6, pp. 3612–3625, June 2022.

[26] B. Tian, L. Liu, H. Lu, Z. Zuo, Q. Zong, and Y. Zhang, "Multivariable finite time attitude control for quadrotor UAV: Theory and experimentation," *IEEE Trans. Ind. Electron.*, vol. 65, no. 3, pp. 2567–2577, Mar. 2018.

[27] S. Kamal, J. A. Moreno, A. Chalanga, B. Bandyopadhyay, and L. M. Fridman, "Continuous terminal sliding-mode controller," *Automatica*, vol. 69, pp. 308–314, Jul. 2016.

[28] X. Liu, M. Zhang, E. Rogers, Y. Wang, and F. Yao, "Terminal sliding mode-based tracking control with error transformation for underwater vehicles," *Int. J. Robust Nonlin. Control*, vol. 31, no. 15, pp. 7186–7206, 2021.

[29] B. Guo, Y. Liu, and L. Liu, "Adaptive neural fault-tolerant control of a quadrotor uav via fast terminal sliding mode", *Aerosp. Sci. Technol.*, vol. 129, pp. 107818, Oct. 2022.

[30] N. P. Nguyen, H. Oh, and J. Moon, "Continuous nonsingular terminal sliding mode control with integral-type sliding surface for disturbed systems: Application to attitude control for quadrotor uavs under external disturbances," *IEEE Trans. Aerosp. Electron. Syst.*, vol. 58, no. 6, pp. 5635–5660, Dec. 2022.

[31] L. Yang and J. Yang, "Nonsingular fast terminal sliding-mode control for nonlinear dynamical systems," *Int. J. Robust Nonlin. Control*, vol. 21, no. 16, pp. 1865–1879, Nov. 2011.

[32] P. Tang, D. Lin, D. Zheng, S. Fan, and J. Ye, "Observer based finite-time fault tolerant quadrotor attitude control with actuator faults", *Aerosp. Sci. Technol.*, vol. 104, pp. 105968, Sept. 2020.

[33] S. D. Xu, C. C. Chen, and Z. L. Wu, "Study of nonsingular fast terminal sliding-mode fault-tolerant control", *IEEE Trans. Ind. Electron.*, vol. 62, no. 6, pp. 3906–3913, June 2015.

[34] A. Jouila and K. Nouri, "An adaptive robust nonsingular fast terminal sliding mode controller based on wavelet neural network for a 2-DOF robotic arm", *J. Frankl. Inst.*, vol. 357, pp. 13259–13282, 2020.

[35] B. Ding, D. Xu, B. Jiang, P. Shi, and W. Yang, "Disturbance-observer-based terminal sliding mode control for linear traction system with prescribed performance," *IEEE Trans. Transp. Electrific.*, vol. 7, no. 2, pp. 649–658, June 2021.

[36] J. Cao, H. X. Li, and D. W. C. Ho, "Synchronization criteria of lur'e systems with time-delay feedback control," *Chaos, Solitons Fractals*, vol. 23, no. 4, pp. 1285–1298, Feb. 2005.

[37] S. Dudzik, "Application of the motion capture system to estimate the accuracy of a wheeled mobile robot localization," *Energies*, vol. 13, no. 23, pp. 1–23, 2020.

[38] A. Astolfi, R. Ortega, and A. Venkatraman, "A globally exponentially convergent immersion and invariance speed observer for mechanical systems with non-holonomic constraints," *Automatica*, vol. 46, no. 1, pp. 182-189, 2010.

[39] W. Wei and W. Zhang, "Command-filter-based adaptive fuzzy finite-time output feedback control for state-constrained nonlinear systems with input saturation," *IEEE Trans. Fuzzy Sys.*, vol. 30, no.10, pp. 4044–4056, Oct. 2022.

[40] Y. Li, Y. Liu, and S. Tong, "Observer-based neuro-adaptive optimized control of strict-feedback nonlinear systems with state constraints," *IEEE Trans. Neural Netw. Learn. Syst.*, vol. 33, no.7, pp. 3131–3145, Jul. 2022.

[41] Q. Hu, B. Jiang, and M. Friswell, "Robust saturated finite time output feedback attitude stabilization for rigid spacecraft," *J. Guid., Control, Dyn.*, vol. 37, no. 6, pp. 1914–1929, 2014.

[42] D. Ye, Y. Xiao, Z. Sun, and B. Xiao, "Neural network based finite-time attitude tracking control of spacecraft with angular velocity sensor failures and actuator saturation," *IEEE Trans. Ind. Electron.*, vol. 69, no. 4, pp. 4129–4136, Apr. 2022.

[43] Y. Sun, C. Zheng, and P. Mercorelli, "Velocity-free friction compensation for motion systems with actuator constraint," *Mech. Syst. Signal Proc.*, vol. 148, pp. 107132, Feb. 2021.

[44] X. -G. Guo and C. K. Ahn, "Adaptive fault-tolerant pseudo-pid sliding-mode control for high-speed train with integral quadratic constraints and actuator saturation," *IEEE Trans. Intell. Transp. Syst.*, vol. 22, no. 12, pp. 7421–7431, Dec. 2021.

[45] K. Eliker, S. Grouni, M. Tadjine, and W. Zhang, "Practical finite time adaptive robust flight control system for quad-copter uavs," *Aerosp. Sci. Technol.*, vol. 98, pp. 105708, Mar. 2020.

[46] X. Hu, G. Zhu, Z. Li, R. Malekian, and M. Á. Sotelo, "Event-triggered adaptive fuzzy setpoint regulation of surface vessels with unmeasured velocities under thruster saturation constraints," *IEEE Trans. Intell. Transp. Syst.*, vol. 23, no. 8, pp. 13463–13472, Aug. 2022.

[47] W. Liu, X. Cheng, and J. Zhang, "Command filter-based adaptive fuzzy integral backstepping control for quadrotor UAV with input saturation," *J. Frankl. Inst.*, vol. 360, pp. 484–507, 2023.

[48] F. Falcón, H. Ríos, and A. Dzul "A robust fault diagnosis for quad-rotors: A sliding-mode observer approach," *IEEE/ASME Trans. Mechatronics*, vol. 27, no. 6, pp. 4487–4496, Dec. 2022.

[49] K. Liu, R. Wang, S. Zheng, S. Dong, and G. Sun, "Fixed-time disturbance observer-based robust fault-tolerant tracking control for uncertain quadrotor UAV subject to input delay", *Nonlinear Dyn.,* vol. 107, pp. 2363–2390, 2022.

[50] S. Harshavarthini, R. Sakthivel, and C. K. Ahn, "Finite-time reliable attitude tracking control design for nonlinear quadrotor model with actuator faults," *Nonlinear Dyn.,* vol. 96, pp. 2681–2692, Apr. 2020.

[51] Y. Xiao, A. D. Ruiter, D. Ye, and Z. Sun, "Adaptive fault-tolerant attitude tracking control for flexible spacecraft with guaranteed performance bounds," *IEEE Trans. Aerosp. Electron. Syst.*, vol. 58, no. 3, pp. 1922-1940, June 2022.

Kang Liu (Member, IEEE) received the Ph.D. degree in control science and engineering from the University of Science and Technology of China, Hefei, China, in 2022.

He is currently a Postdoctoral Researcher with the Department of Computer Science, University of Sheffield, Sheffield, U.K.. His research interests include theoretical researches and engineering applications in intelligence control algorithms and precision agriculture systems, such as deep learning, fuzzy control and neural networks for unmanned aerial vehicles, spacecraft dynamics, and autonomous vehicles, drone remote sensing, agricultural big data, and pest and disease identification.

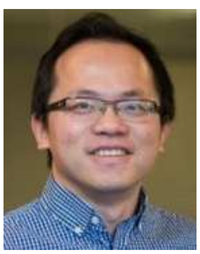

Po Yang (Senior Member, IEEE) received the B.Sc. degree in computer science from Wuhan University, Wuhan, China, in 2004, the M.Sc. degree in computer science from Bristol University, Bristol, U.K., in 2006, and the Ph.D. degree in electronic engineering from the University of Staffordshire, Stafford, U.K., in 2011.

He is currently a Senior Lecturer in Largescale Data Fusion with the Department of Computer Science, University of Sheffield, Sheffield, U.K. He is a Postdoctoral Research Fellow with the Department of Computing, Bedfordshire University, Luton, U.K. Before he was with the Bedfordshire University, he was a Research Assistant with the University of Salford. His main research interests include radio-frequency identification and sensor networking, document image processing, computer vision, GPU, and parallel computing.

Rujing Wang received the B.E. degree in computer science from the Huazhong University of Science and Technology, Wuhan, China, in 1987, the M.S. degree in electronic engineering from the Dalian University of Technology, Dalian, China, in 1990, and the Ph.D. degree in pattern recognition and intelligent system from the University of Science and Technology of China, Hefei, China, in 2005.

He is currently with the Institute of Intelligent Machines, Chinese Academy of Sciences, as a Professor and a Researcher. His current research interests include intelligent agriculture, the agricultural Internet of Things, and agricultural knowledge engineering.

Lin Jiao (Member, IEEE) received the Ph.D. degree in computer science and technology from the University of Science and Technology of China, Hefei, China, in 2021.

She is currently a lecturer with the School of Internet, Anhui University, Hefei, China. She has published over 20 papers and served as a reviewer for more than 10 journals/conferences. Her research interests include machine learning, deep learning, patter recognition, and computer vision.

Tao Li (Member, IEEE) was born in Wuhan, China, 1981. He received the B.S. degree from Wuhan Institute of Technology, Wuhan, China, in 2004, the Master's degree from Central China Normal University, Wuhan, China, in 2007, and Ph. D. degree from Central South University, Changsha, China, in 2017. He was a Postdoctoral Fellow at CRRC Zhuzhou Institute Co., Ltd. from 2017 to 2020.

Now he is an Associate Professor at Hunan University of Technology. His main research interests include nonlinear systems, machine learning and intelligent control.

Jie Zhang received the M.S. degree from the Hefei University of Technology, in 2009, and the Ph.D. degree from the University of Science and Technology of China, in 2014.

He is with the Institute of Intelligent Machines, Hefei Institutes of Physical Science, Chinese Academy of Sciences, where he is currently an Associate Professor. His current research interests include image processing, pattern recognition, and artificial intelligence.